

**Image Analysis for Mandible Bone Properties on
Cone-Beam CT to Detect Osteoporosis**

تحليل الصور لخواص عظام الفك السفلي في الصور المخروطية ثلاثية
الابعاد للكشف عن هشاشة العظام

Prepared by

Rasha Abu Marar (401710081)

Supervisor: Prof. Hamza Abbass Al-Sewadi

Master Thesis

Submitted in Partial Fulfillment for the Requirements of the

Master Degree in Computer Science

Faculty of Information Technology

Middle East University

May 2019


Authorization

I, **Rasha Fathi Abu Marar**, authorize Middle East University to provide hard copies or soft copies to libraries, institutions and establishments upon request.

Name: Rasha Fathi M. Abu Marar

Date: 14/6/2019

Signature:



Dr. Rasha Fathi M. Abu Marar (Member / Chairman)
Associate Professor, Department of Computer Science
Middle East University (MEU)

Dr. Adnan Badr M. Al-Hilali (External Examiner)
Associate Professor, Department of Computer Science
MEU

Thesis Committee Decision

This thesis titled " **Image Analysis for Mandible Bone Properties on Cone-Beam CT to Detect Osteoporosis**" was successfully defended and approved on 29/5/2019.

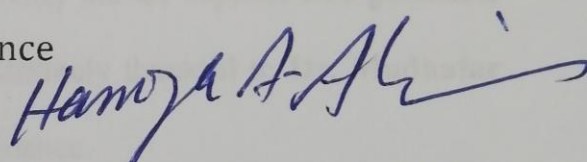
Thesis Committee Members

Signature

(Prof. Hamza Abbass Al-Sewadi (Supervisor))

Professor, Department of Computer Science

Middle East University (MEU)

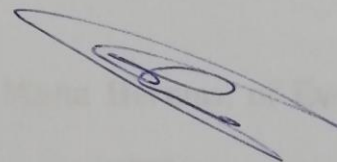


15-6-2019

DR. Mudhafar Al-Jarrah (Member/ Chairman)

Associate Professor, Department of Computer Science

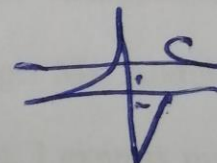
Middle East University (MEU)



DR. Adnan Hadi M. Al-Hilali (External Examiner)

Associate Professor, Department of Computer Science

Isra University



هذا من فضل ربي

Acknowledgment

First, praises and thanks to **ALLAH**, for His showers of blessings throughout my research work to complete the research successfully.

I would like to express my deep and sincere gratitude to my research supervisor **Prof. Hamza Abbass Al-Sewadi** for the continuous support of my MSc. study and research, for his patience, motivation, and immense knowledge. His guidance helped me in all the time of research and writing of this thesis.

I respect and thank **Dr. Diao Uliyan**, for giving me all support and guidance, which made me complete the project duly. I am extremely thankful to **Dr. Mudhafar Al-Jarrah** for providing such a nice support and guidance.

I owe my deep gratitude to our **Dr. Abeer Al-Hadidi**, from Jordan University who took keen interest on our project, till the completion of my project work by providing all the necessary medical information.

I would not forget to remember **Belal Ayasra** and **Muna Hermas**, of Everest Radiology Center who support me with CBCT images and DEXA examination throughout the project work. I would like to say thanks to my job manager **Mr. Abdelmotaleb Al-nugrush** and colleagues, for their constant encouragement. I express my special thanks **Mr. Nidal Hamdan**, for his technical support throughout this research work.

Finally, thanks go to all the people who have supported me to complete the research work directly or indirectly.

Dedication

I dedicate this thesis to my family for their love, prayers, caring and sacrifices for educating and preparing me for my future. I am very much thankful to my husband **Mohammed AL- Ostah** and my children's **Leen, Lana** and **Hasan** for their love, understanding, prayers and continuing support to complete this research work.

I also dedicate this work to my **parents, sisters** and **brothers**, for their support and valuable prayers. Last to **my friends** who shown keen interest to complete this thesis successfully.

Table of Content

| | |
|--------------------------------------------------|--------------|
| Cover Page | I |
| Authorization | II |
| Thesis Committee Decision | III |
| Acknowledgment | IV |
| Dedication | V |
| Table of Content | VI |
| List of Tables | X |
| List of Figures | XI |
| List of Appendices | XIII |
| List of Abbreviations | XIV |
| Abstract | XVI |
| المخلص | XVIII |
| 1 CHAPTER ONE | 1 |
| BACKGROUND AND THE STUDY IMPORTANCE | 2 |
| 1.1 Introduction | 2 |
| 1.2 Definitions | 3 |
| 1.2.1 Image Analysis..... | 3 |
| 1.2.2 Mandible Bone | 3 |
| 1.2.3 Osteoporosis | 3 |
| 1.2.4 Cone Beam Computed Tomography (CBCT) | 4 |

| | | |
|------------|---------------------------------------------------------------|----------|
| 1.3 | Problem Statement | 5 |
| 1.4 | Research Questions..... | 5 |
| 1.5 | Objectives of the Study..... | 6 |
| 1.6 | Motivation | 6 |
| 1.7 | Contribution and Significance of the Research..... | 7 |
| 1.8 | Scope and Limitations | 7 |
| 1.9 | Thesis Outline | 7 |
| 2 | CHAPTER TWO..... | 8 |
| | THE THEORETICAL BACKGROUND AND LITERATURE REVIEW | 9 |
| 2.1 | Overview..... | 9 |
| 2.2 | Introduction | 9 |
| 2.3 | Background | 9 |
| 2.3.1 | Computed Tomography..... | 10 |
| 2.3.2 | Bone Tissue | 10 |
| 2.3.3 | Osteoporosis Detection Techniques | 12 |
| 2.3.4 | Overview of the DICOM..... | 13 |
| 2.3.5 | BMC & BMD Measurements..... | 14 |
| 2.3.6 | Anatomic Landmarks in Maxillofacial Region. | 14 |
| 2.3.7 | Why Mandible Bone?..... | 15 |
| 2.3.8 | Trabecular bone texture features | 16 |
| 2.3.9 | Image Processing and Artificial Neural Networks | 16 |
| 2.3.10 | Fundamental Steps in Image Processing:..... | 18 |
| 2.3.11 | Edge Detection..... | 20 |

| | | |
|------------|-----------------------------------------------------|-----------|
| 2.3.12 | Features Extraction | 24 |
| 2.3.13 | Classification..... | 31 |
| 2.4 | Related Work | 32 |
| 2.5 | Summery..... | 44 |
| 3 | CHAPTER THREE..... | 46 |
| | METHODOLOGY AND THE PROPOSED TECHNIQUE | 46 |
| 3.1 | Overview..... | 46 |
| 3.2 | Introduction | 46 |
| 3.3 | Materials..... | 46 |
| 3.4 | Methodology and Design..... | 47 |
| 3.4.1 | Image Processing..... | 48 |
| 3.4.2 | Feature Extraction | 51 |
| 3.4.3 | Classification | 52 |
| 3.4.4 | Training Phase..... | 56 |
| 3.4.5 | Testing Phase..... | 56 |
| 3.5 | Summary | 57 |
| 4 | CHAPTER FOUR | 59 |
| | DESIGN, IMPLEMENTATIOM, AND TESTING..... | 59 |
| 4.1 | Overview..... | 59 |
| 4.2 | Introduction | 59 |
| 4.3 | Dataset | 59 |

| | | |
|------------|-----------------------------------------------|-----------|
| 4.4 | Implementation | 60 |
| 4.4.1 | Gaussian Filter..... | 60 |
| 4.4.2 | Binarization | 61 |
| 4.4.3 | Edge Detection | 61 |
| 4.4.4 | Segmentation..... | 67 |
| 4.4.5 | Filtering Effect and Feature Extraction | 67 |
| 4.4.6 | Classification..... | 70 |
| 4.5 | Experimental Results | 70 |
| 4.5.1 | Data Analysis | 70 |
| 4.6 | Summery | 73 |
| 5 | CHAPTER FIVE | 76 |
| | CONCLUSION AND FUTURE WORK | 75 |
| 5.1 | Conclusion | 76 |
| 5.2 | Future Work: | 77 |
| | REFERENCES | 79 |
| | APPENDIX A | 83 |
| | APPENDIX B | 86 |
| | APPENDIX C | 89 |

List of Tables

| Chapter Number. Table Number | Contents | Page |
|---------------------------------|-------------------------------------------------------------|------|
| Table 2.1 | Comparison Between Normal and Osteoporotic Bone. | 16 |
| Table 2.2 | Comparison Between related work | 22 |
| Table 3.1 | Definitions of the Used Dataset Variables as Input. | 52 |
| Table 3.2 | The Architecture and Parameters of the Designed NN. | 55 |
| Table 4.1 | Feature Extraction from Original Image. | 69 |
| Table 4.2 | Feature Extraction After Image Pre-Processing. | 69 |
| Table 4.3 | Definitions of the Used Dataset Variables as Input. | 71 |
| Table 4.4 | The BP-ANN Classifier performance investigation | 72 |
| Table 4.5 | Cross-Entropy for The NN as a Function of Number of Epochs. | 73 |

List of Figures

| Chapter Number. Table Number | Contents | Page |
|---------------------------------|------------------------------------------------------------------------|------|
| Figure 1.1 | Cone-Beam CT System | 5 |
| Figure 2.1 | Definition of Bone Structure Parameters | 12 |
| Figure 2.2 | Temporomandibular Joints are seen on Coronal, Sagittal and Axial Views | 15 |
| Figure 2.3 | Mental Foramen | 15 |
| Figure 2.4 | The Image Processing Chain | 17 |
| Figure 2.5 | Image Processing Steps | 18 |
| Figure 2.6 | Types of Edge Detector | 22 |
| Figure 2.7 | Block Diagram of Image Enhancement Using Canny Edge Detector | 24 |
| Figure 2.8 | Fine Textures Have Smaller Coarsness Value than the Coarse Ones | 27 |
| Figure 2.9 | Different Contrast | 28 |
| Figure 2.10 | Two Images Differs the Orientation | 29 |
| Figure 2.11 | Sigmoidal function. | 33 |
| Figure 2.12 | The Selected Coronal Slice After Angulation Adjustment of CBCT Image | 35 |
| Figure 3.1 | Proposed System | 47 |
| Figure 3.2 | Mandible Slice Where Both Foramina Appear Simultaneously | 48 |
| Figure 3.3 | Block Diagram of Image Pre-processing Steps | 49 |
| Figure 3.4 | Flow Chart of Canny Edge Detection Algorithm | 50 |
| Figure 3.5 | Architecture of NN (7:15:1) | 54 |
| Figure 3.6 | Training the Back- Propagation Neural Network | 56 |

| Chapter Number. Table Number | Contents | Page |
|-------------------------------------|--------------------------------------------------------------------|-------------|
| Figure 3.7 | Testing Phase Steps | 56 |
| Figure 4.1 | The Result of Applying Gaussian Filter | 61 |
| Figure 4.2 | Edge Detection Using Matlab2018b Roberts Edge Detection | 62 |
| Figure 4.3 | Sobel Edge Detection Using Matlab2018b | 63 |
| Figure 4.4 | Edge Detection Using Matlab2018b Prewitt Edge Detection | 64 |
| Figure 4.5 | Edge Detection Using Canny on Matlab 2018b | 65 |
| Figure 4.6 | Edge Detection Using Canny Edge Detection With Specified Threshold | 66 |
| Figure 4.7 | Segmented Image | 67 |
| Figure 4.8 | Architecture of B-PANN (7:15:1) | 70 |
| Figure 4.9 | Confusion Matrix For Classification | 71 |
| Figure 4.10 | Validation Performance | 73 |

List of Appendices

| Appendix Number | Contents | Page |
|------------------------|----------------------------------------------|-------------|
| Appendix A | DEXA Scan For Normal Patient x | 83 |
| Appendix B | DEXA Scan For Osteoporotic Patient y Page 1. | 86 |
| Appendix C | Images Features Data Set | 89 |

List of Abbreviations

| Abbreviation | Meaning |
|--------------|-----------------------------------------------|
| AC | Alternation Current |
| ANN | Artificial Neural Network |
| BDMC | Bone Density of Mandibular Condyle |
| BMC | Bone Mineral Content |
| BMD | Bone Minerals Density |
| BP-ANN | Back Propagation Artificial Neural Network |
| CBCT | Cone-Beam Computed Tomography |
| CT | Quantitative Computed Tomography |
| CTI | Computed Tomography Indices |
| CTI(I) | computed tomography mandibular index inferior |
| CTI(S) | mandibular index superior |
| CTMI | Computed tomography mental index |
| DC | Direct Current |
| DCT | Discrete Cosine Transform |
| DEXA | Dual-Energy X-ray Absorptiometry |
| DICOM | Digital Imaging and Communication in Medicine |
| FD | Fractal Dimension |
| FoV | Field of View |
| HA | Histogram Analysis |
| HU | House Field Unit |
| LoG | Laplacian of Gaussian |

| abbreviation | Meaning |
|---------------------|----------------------------|
| MI | Mental Index |
| PAN | Panoramic Radiography |
| PMI | Panoramic Mandibular Index |
| RD | radiographic density |
| RoI | Regions of Interest |
| Tb.N | Trabecular Number |
| Tb.Nd | Trabecular Nodes |
| Tb.Sp | Trabecular Separation |
| Tb.Th | Trabecular Thickness |
| Tb.Tm | Trabecular Termini |
| Vol | Volume of Interest |
| WHO | World Health Organization |

Image Analysis for Mandible Bone Properties on Cone-Beam CT to Detect Osteoporosis

Prepared by

Rasha Abu Marar

Supervisor

Prof. Hamza Abbass Al-Sewadi

Abstract

Osteoporosis is common in the elderly and the dentist is often the most healthcare professional that they visit regularly. The aim of this study is to detecting osteoporosis using cone beam computed tomography (CBCT images) in order to reduce the risk of jaws fracture and dental implant failure, and looking forward to create an opportunity for early osteoporosis detection, and timely diagnosis, in addition to treatment cost reduction. Fast computers and artificial intelligence provide excellent tool to serve this purpose.

A set of mandibles CBCT image slices samples for 50-85 years old women that will be obtained from patients' data that consist of CBCT and bone minerals density (BMD) information that were already determined by dual-energy X-ray absorptiometry (DEXA). These sample images were anonymously supplied from local digital radiology centers using highly sophisticated modern radiographic equipment.

The obtained patients CBCT images will be assigned into two groups; osteoporosis and healthy (normal), using the T-score derives from the DEXA technique. Professional physicians already did the medical diagnosis. The diagnosis algorithm proposed in this

paper is designed for automatic detection of Osteoporosis in CBCT images. The approach is based on image processing, feature extraction and artificial neural network (ANN) technology. Employing feed forward back-propagation classifier has successfully allowed for osteoporosis detection from CBCT images. Seven parameters were involved in the experiment data preparation as input; the author introduces four of them in order to increase the decision accuracy.

For classification a database of 120 CBCT image slices, which are organized in two classes of 60 images that include both normal and osteoporotic cases, 72 images used for training and 48 images used for testing.

The obtained research performance of the classification algorithm for the osteoporosis occurrence in the test samples used is evaluated using four metrics, namely; precision, recall, accuracy rate, and F1-score, which resulted into 0.96, 1, 97.917%, and 0.97959, respectively.

The designed classifier converges to the acceptable level using a best validation performance of $5.5761e-08$. The results demonstrate the effectiveness of the proposed algorithm. With the help of the proposed method, dentists will be able to predict osteoporosis accurately and efficiently without the need for further examination by the painful and costly DEXA examination. This means a great relief on reducing the risk of jaws fracture and dental implant failure.

Keywords: Artificial Intelligence, Neural Networks Classifiers, Osteoporosis, Cone-Beam CT, Image processing.

تحليل الصور لخواص العظام الفكية في الصور المخروطية ثلاثية الابعاد

للكشف عن هشاشة العظام

إعداد: رشا فتحي أبو مرار

إشراف: أ.د. حمزة عباس السوادي

الملخص

مرض هشاشة العظام شائع بين كبار السن. تهدف هذه الدراسة الى الكشف المبكر عن هشاشة العظام باستخدام تحليل الصور لخواص العظام الفكية في الصور المخروطية ثلاثية الابعاد (CBCT). وكذلك من أجل الحد من خطر الاصابة بكسور الفك والفشل في زراعة الأسنان. هذا بالإضافة إلى تقليل الكلف المترتبة على العلاج نظراً لكون أجهزة الكمبيوتر السريعة والذكاء الاصطناعي تعتبر أداة مميزة لخدمة هذا الغرض.

مجموعة من عينات صور CBCT للفك السفلي للنساء في عمر ما بين 50-85 سنة ومعلومات كثافة المعادن العظمية (BMD) التي تم تحديدها بالفعل بواسطة فحص (DEXA) التي تم الحصول عليها من بيانات المرضى، وقد تم توفير هذه الصور من خلال مركز افرست للأشعة الذي يقوم باستخدام معدات التصوير الشعاعي الحديثة والمتطورة.

وتم تقسيم صور ((CBCT)) للمرضى الذين تم الحصول على صورهم في مجموعتين؛ الاولى المصاب

بهشاشة العظام والثانية غير مصاب بهشاشة العظام وذلك باستخدام (T-score) المستمدة من تقنية (DEXA).

وقد تم التشخيص الطبي بالفعل من قبل الأطباء المختصين، وتم تصميم خوارزمية التشخيص المقترحة

في هذا البحث للكشف التلقائي عن مرض هشاشة العظام في صور (CBCT).

ويعتمد النهج على معالجة الصور واستخراج المعالم والتصنيف باستخدام تكنولوجيا الشبكة العصبية

الاصطناعية. وقد ساعد استخدام مصنف إعادة الانتشار إلى الأمام (B-PANN) على الكشف بنجاح عن هشاشة

العظام من خلال صور CBCT. وقد تم اعتماد سبع خصائص في إعداد بيانات التجربة كمدخلات، أربعة منها

مقدمة من قبل الباحث.

للتصنيف قاعدة بيانات مكونة من 120 صورة مقسمة إلى صنفين مريض وسليم بالتساوي، 72 صورة

استخدمت لتدريب الشبكة العصبونية، و 48 صورة استخدمت للتجربة.

و قد تم تقييم نتائج البحث التي تم الحصول عليها من خوارزمية تصنيف حدوث هشاشة العظام في

عينات الاختبار المستخدمة باستخدام أربعة مقاييس هي؛ الدقة، الاستدعاء، معدل الدقة و **F1-score** ، وقد

اظهرت النتائج القيم التالية لهذه المقاييس: 0.96 ، 1 ، 97.917% ، 0.97959 على التوالي.

ويتقارب التصميم إلى المستوى المقبول ويستخدم أفضل أداء تحقق من $5.5761e-08$. وتوضح النتائج

فعالية الخوارزمية المقترحة. وبمساعدة الطريقة المقترحة سيكون أطباء الأسنان قادرين على التنبؤ بمرض هشاشة

العظام بدقة وكفاءة دون الحاجة إلى مزيد من الفحص بواسطة الفحص **DEXA**، وهذا يعني راحة كبيرة للمريض،

وتقليل التكاليف المادية والحد من مخاطر كسر الفك وفشل زراعة الأسنان.

CHAPTER 1

Background and the Study

Importance

Chapter One

Background and the Study Importance

1.1 Introduction

Osteoporosis is common in the elderly and the dentist is often the most healthcare professional that they visit regularly. The risk of jaws fracture and dental implant failure is very high when osteoporosis exists.

Osteoporosis refers to both, decreased bone mass and micro-architectural deterioration of the bone scaffold (Güngör, Yildirim & Çevik, 2016). Complications of osteoporosis such as osteoporotic fracture are associated with high morbidity and medical costs. The risk for such complications can be reduced if the disease is diagnosed and treated earlier (Alkhader, Aldawodyeh & Abdo, 2018). Cone-beam computed tomography (CBCT) has been widely accepted in dentistry since its introduction in 1998 (Barngkegi, Joury, & Jawad, 2015). Dual-energy X-ray Absorptiometry (DEXA) is the most common technique for obtaining osteoporosis (Esmaeli, Payahoo, Mobasseri, Johari, & Yazdani, 2017). DEXA is not always available and it is not considered as cost-effective tool for screening in low-risk patients, such as younger individuals (Alkhader et.al. 2018). The aim of this study is to use CBCT images in the prediction of osteoporosis in mandible bone. Many of the useful image processing techniques will be used to enhance the CBCT images in order to extract useful features that will assist in the classification process. Then one of the artificial intelligence techniques will be utilized and adjusted for the detection and diagnoses of the osteoporosis from the examination of mandible CBCT images.

1.2 Definitions

This section lists brief definitions for the most important words or phrases that are relevant to the field studied in this thesis.

1.2.1 Image Analysis

Extracting any distinguishable attributes from images, up to and including the recognition of individual objects (Gonzalez & Woods, 2018).

This analysis is mainly used for digital images. To be able to extract different components from an image data set. The data must be preprocessed to find different shapes or edges, remove noise and/or measure properties of an object. As example, image enhancement includes noise removing, and image segmentation in order to isolate and distinguish objects or regions of interest (RoI) (Klintström, 2017).

1.2.2 Mandible Bone

The mandible, or lower jaw, is the bone that forms the lower part of the skull, and along with the maxilla (upper jaw), forms the mouth structure (Healthline 2018). Movement of the lower jaw opens and closes the mouth and allows for the chewing of food. The lower set of teeth in the mouth is rooted in the lower jaw (American bone health 2018).

1.2.3 Osteoporosis

Osteoporosis—Osteo (bones) and porosis (porous) means porous bones (Kannan & Kumar, 2015). Osteoporosis is a systemic disease characterized by a low bone mass, deterioration of the bone structure, and increased bone fragility. Bone loss occurs with aging after approximately the age of 30 years (Koh & Kim, 2011). Osteoporosis is a major health problem and affects a significant number of people (Beatriz, Cal & Aranha, 2016).

Most of the cases are in women (90%), with Caucasian and Asian women at the highest risk. African-American and Latina women are at a lower but still significant risk (Barngkgei, Haffar & Khattab, 2014).

One-third of the women diagnosed with osteoporosis develop a fracture within five years. Hence, early diagnosis can improve the prognosis and the quality of life of patients; however, the silent nature of this disease may delay the diagnosis until fractures occur. It has been estimated that the annual medical costs for management of acute fractures and rehabilitation range is between US\$ 17 to 20 billion. In addition, there are indirect monetary and nonmonetary costs (e.g., care time) that add to the financial and social burden of this disease (Barngkgei et.al, 2015).

1.2.4 Cone Beam Computed Tomography (CBCT)

Cone beam computed tomography (CBCT) might be one of the most important developments in dental radiology over the years. The first prototype scanner for CBCT was developed and described in 1982 for angiographic applications (Mayil, Keser, & Pekiner, 2014). Recently, CBCT technique has been introduced to dentistry, which is able to provide 2D and 3D images with tools for measuring bone density (Esmaeli et. al., 2017). Cone-beam geometry immediately captures a two dimensional image through a three dimensional X-ray beam, which scans the shape of a cone.

The X-ray tube and detector rotate around the object of interest, as displayed in Figure 1.1. This three-dimensional beam proves efficient as at most one rotation around the object provides enough information to reconstruct a three-dimensional image.

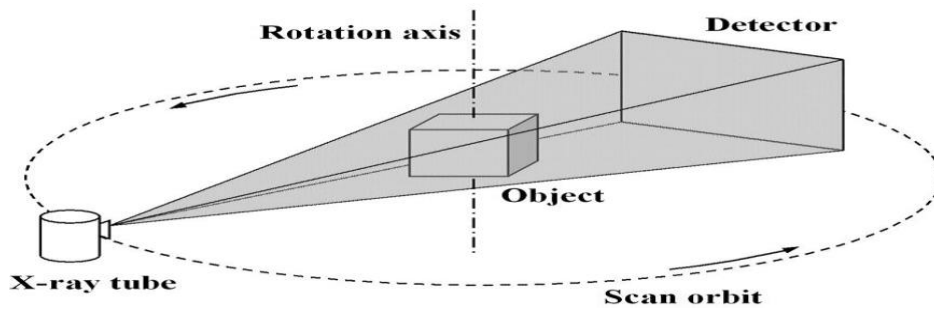


Figure 1.1: Cone-Beam CT System (Held, & Bauer, 2017).

1.3 Problem Statement

Current CBCT devices do not produce calibrated house field unit values (HU). They only produce a kind of grey-scale values. Some studies suggest that CBCT resulting values may be reliable, but these values differ for different devices as well as they vary according to the placement of the object in the imaged field of view (FoV) (Klintström, 2017). Moreover, despite the ability to detect bone density and the quality of structures by this technique, few studies have been conducted on the use of house field unit values (HU) in detecting osteoporosis, so it cannot be argued with certainty about detective values of house field unit values (HU). Hence, what would be the features combination that gives the ability to detect osteoporosis from CBCT images is still hot subject and needs further study. Besides a search for a more rigid and reliable techniques, would serve to enhance osteoporosis diagnosis.

1.4 Research Questions

- What would be the features combination that gives an accurate features value of the CBCT to detect osteoporosis?
- What new features parameters in CBCT may be added to increase accuracy?
- How accurate is to detect osteoporosis from CBCT of mandible accurately using image processing techniques and ANN?

1.5 Objectives of the Study

The main objectives of this study are:

- To develop an algorithm that utilizes image processing and ANN techniques in order to detect osteoporosis from region of interest on cone beam CT based on feature extraction algorithm.
- To analyze pattern of bone loss in the CBCT image, then estimating mandibular trabecular nodes (Tb.Nd), trabecular termini (Tb.Tm), trabecular separation (Tb.Sp), trabecular number (Tb.N), Trabecular spacing (Tb.Sc), Bone volume over total volume (BV/TV) and trabecular thickness (Tb.Th), to create a features vector.
- To classify CBCT images into two categories, namely normal patient or osteoporotic patient using ANN classifier.

1.6 Motivation

This research is motivated by the need to the silent nature of osteoporosis-delayed diagnosis, and looking forward to create an opportunity for early detection, and timely diagnosis.

Osteoporosis is common in the elderly and the dentist is often the only healthcare professional that they visit regularly. Since CBCT is widely used for routine examinations when planning treatment, this study evaluates whether the presence of osteoporosis might be apparent in a population of patients who underwent CBCT. Dental radiographic density may be useful in clinical dental practice to identify osteoporotic women with previously undetected low bone minerals density (BMD).

1.7 Contribution and Significance of the Research

Detecting osteoporosis using CBCT images reduces the risk of jaws fracture and dental implant failure, and looking forward to create an opportunity for early osteoporosis detection, and timely diagnosis, in addition to treatment cost reduction.

1.8 Scope and Limitations

The scope of the proposed method is medical image processing. This study evaluates whether the presence of osteoporosis might be apparent in a population of patients mandible who underwent CBCT.

The research is limited to give accurate results of the mandibular bone quality in-patient who never takes Bone density enhancement drugs.

1.9 Thesis Outline

This chapter provided an overview about dental view about osteoporosis. The research problem, objectives, limitations, and scope are also discussed. The rest of this thesis is organized as follows:

Chapter Two discusses and reviews the previous studies that are related to osteoporosis detection using various techniques.

Chapter Three presents methodology and the proposed technique used for the diagnosis of osteoporosis by the aid of CBCT images.

Chapter Four presents the implementation of the proposed method. Results are also listed and discussed in this chapter.

Chapter Five will give a general summary of the thesis, summarizing the research findings and suggesting related future works.

CHAPTER 2

The Theoretical Background and Literature Review

Chapter Two

The Theoretical Background and Literature Review

2.1 Overview

This chapter presents details of the approaches that are used to detect osteoporosis. Section 2.2 presents an introduction. Section 2.3 explains the background to understand osteoporosis and its detection techniques. Section 2.4 shows different related work 2.5 presents overall summary of related work.

2.2 Introduction

Early diagnosis of any disease is essential; however, the silent nature of osteoporosis delays its diagnosis. Health care professionals should collaborate to create an opportunity for early detection, timely diagnosis, and start appropriate treatment.

The present research aims to study the changes in the jawbones by investigating images of the advanced imaging technique (CBCT) among women with osteoporosis and those without.

This chapter presents first detailed definitions and theoretical background on the subject of osteoporosis diagnosis and means of investigations. Then a comprehensive literature review and related work for detection of osteoporosis using CBCT of mandible bone is included.

2.3 Background

This section will explain the literature reviews to understand the research topic.

2.3.1 Computed Tomography

It is a technique that attempts to reconstruct the 3-D density of a certain body (volume) by analyzing many 2-D projections of that volume at different angles (Fontaine & Lee, 2002).

Here, the volume of interest (VoI) consists of a cylindrical 3-D region of space. It is represented digitally on a computer as a 3-D array of voxels volume elements containing the value of the density at each small cubical region of the volume. Since X-rays are typically used in practice to generate the projections, the voxels actually hold the amount of X-ray attenuation, not the material density. The X-rays are originated at the projection source, travel through the VoI, and hit a detector opposite the projection source (Fontaine et.al. 2002), as shown in figure 1.1 given in chapter one.

Each projection is stored digitally on the computer as a 2-D array of Texel's texture elements containing the total attenuation of each ray through the VoI. The essential step to reconstruct the original image is back projection by taking each projection and smearing its values back over the VoI along the paths of the original X-rays.

CBCT images are originally gray scale image, In a gray scale image any particular pixel takes an intensity value lying between 0 to 255 (Roy, 2013).

2.3.2 Bone Tissue

Bone tissue is an active, metabolic organ where remodeling takes place throughout the whole life span (Rice, Price, Morley & Beale, 2015). It can be divided into two parts; cortical and trabecular.

2.3.2.1 Cortical Bone

The cortical bone is dense, solid and contains high amounts of mineral. Cortical bone is synonymous to compact bone. Only the periosteal (outside of the cortical bone) and the endosteal (inside of the cortical bone) were considered to be of interest for bone remodeling (Klintström 2017).

2.3.2.2 Trabecular Bone

The inner, trabecular part of trabecular bone can rapidly adapt to mechanical loading and optimize its structure in order to be able to bear high loads with as little tissue as possible. It is therefore of high importance to ascertain how to image and measure the structure of the trabecular bone. The important structure parameters to measure are the following that can be seen as shown in Figure 2.1 (Klintström, 2017).

1. Trabecular nodes (Tb.Nd); are the number of trabecular intersections per mm^3 (mm: millimeter).
2. Trabecular termini (Tb.Tm); are the number of free ends of trabeculae per mm^3 .
3. Trabecular separation (Tb.Sp); is the thickness of the spaces between the trabeculae in mm.
4. Trabecular spacing (Tb.Sc); is the distance between the midlines of the trabeculae in mm.
5. Trabecular thickness (Tb.Th); is the thickness of the trabecular structures (in mm).
6. Trabecular number (Tb.N); are the number of trabeculae in 1 mm^3 (not illustrated in Figure 2.1).

7. Bone volume over total volume (BV/TV); is measured by dividing the number of voxels classified as bone by the total number of voxels in the volume (not illustrated in Figure 2.1).

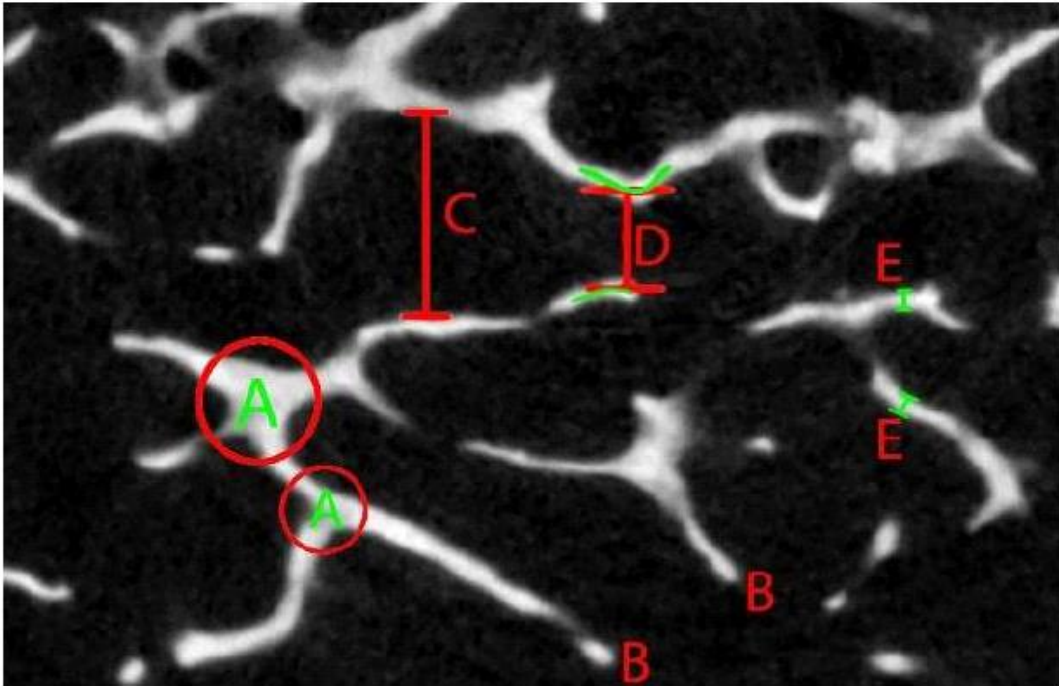


Figure 2.1: Definition of Bone Structure Parameters. Trabecular nodes (A). Trabecular termini (B). Trabecular separation (C). Trabecular spacing (D). Trabecular thickness (E) (Klintström, 2017).

2.3.3 Osteoporosis Detection Techniques

There are many techniques that physician use to detect osteoporosis. This section will describe briefly some of the most relevant to the proposed research work.

2.3.3.1 Dual-energy X-ray Absorptiometry (DEXA)

It is the most common technique for obtaining bone mineral content (BMC) and bone mineral density (BMD) which are often used in the assessment of central bone such as the lumbar spine and hip (Esmaeli et.al., 2017). Although DEXA is used extensively because of its reliability and low radiation dose, it is not always available and it is not

considered as cost-effective tool for screening in low-risk patients, such as younger individuals (Alkhader et.al, 2018).

According to the world health organization (WHO) criteria, individuals with DEXA measurements of the hip or the lumbar spine that yielded T-scores of less than -2.5 were diagnosed with osteoporosis, individuals with T-scores between -1.0 and -2.5 were diagnosed with osteopenia, and participants with T-scores of -1 or greater were considered to have normal bone density (Güngör et. al., 2016).

2.3.3.2 Quantitative Computed Tomography (CT)

It is a technique used instead of DEXA to diagnose osteoporosis, but it is also expensive and associated with higher radiation dose, thus would not be appropriate as screening tool too (Alkhader et.al. 2018).

2.3.3.3 Panoramic Radiograph

Panoramic mandibular index (PMI) on panoramic radiograph has been used to assess the mandibular bone quality. Measurement of the cortical width and a subjective assessment of cortical porosity on panoramic radiographs are methods used previously to diagnose osteoporosis (Koh et. al., 2011). However, the assessment of this test is not so accurate and dentists would not rely on it on its own.

2.3.4 Overview of the DICOM

Digital imaging and communication in medicine (DICOM) is a standard that specifies a non-proprietary data exchange protocol. It consists of several layers in relation to OSI network model. Image displaying under DICOM Standard does not define how images are displayed or annotated. DICOM supports multi-dimensional multi-frame images. Data compression relies on widely used compression standards like JPEG, JPEG

Lossless, JPEG 2000, or MPEG-2 for multi-image (video) sequences. Different medical applications require different levels of image quality (Mustra, Delac and Grgic, 2008).

2.3.5 BMC & BMD Measurements

There are many parameters that can be used to measure the mineral contents in the bones. Two of the widely used parameter are listed below.

2.3.5.1 Bone Mineral Content (BMC)

A measurement of bone mineral found in a specific area. BMC is measured in grams (g) (Gijsbert & van der, 2011).

2.3.5.2 Bone Mineral Density (BMD)

It represent the amount of minerals measured in (grams) per square centimeter (g/cm^2). BMD is derived using BMC divided by area, where BMC is measured in grams (g) and area is measured in square centimeters (cm^2) (Tinoco & Gomez, 2017).

2.3.6 Anatomic Landmarks in Maxillofacial Region.

It is worth looking at the CBCT images for landmarks in maxillofacial region Figure 2.2 shows some Anatomic Landmarks in mandible, joints that are seen on the coronal, sagittal, and axial views (Esmaeli et.al. 2017).

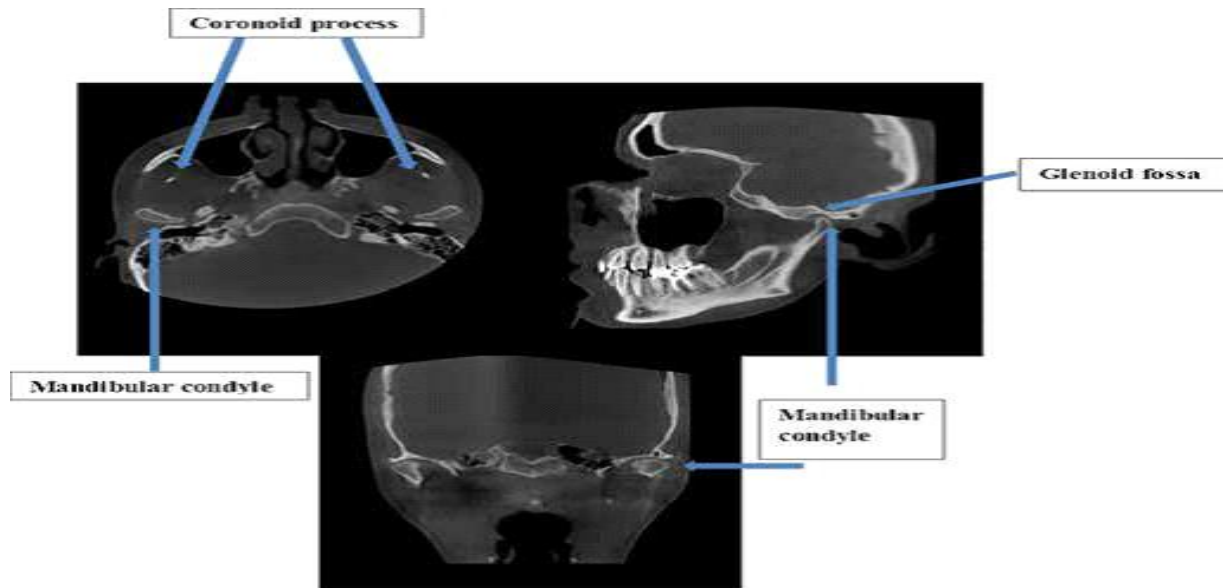


Figure 2.2: Temporomandibular Joints are seen on Coronal, Sagittal and Axial Views (Esmaeli et.al. 2017).

Moreover, the mental foramen can also be illustrated as shown in Figure 2.3 (Rice et.al. 2015).

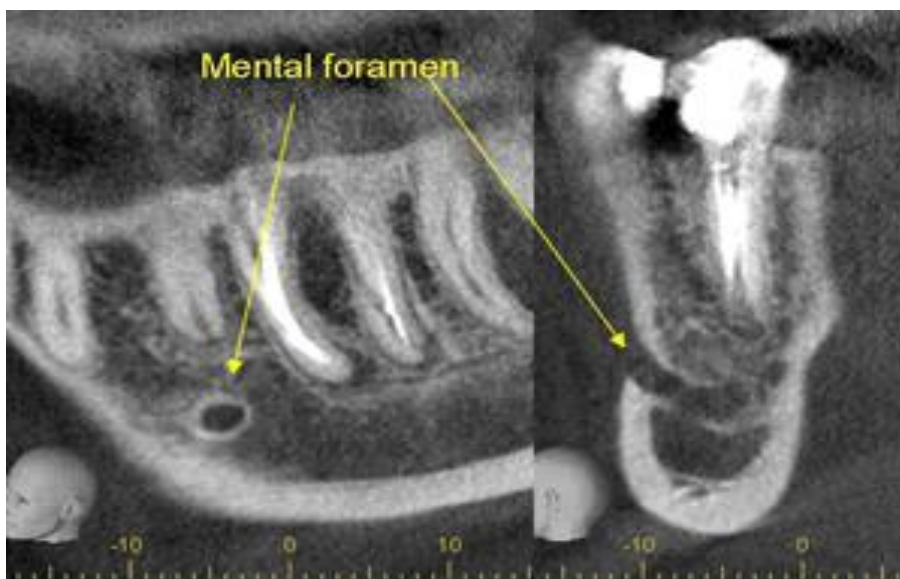


Figure 2.3: Mental Foramen (Rice et.al. 2015) .

2.3.7 Why Mandible Bone?

Due to the morphology of trabecular pattern in anterior mandible based on radiographic studies, and the digital extraction site by morphological filter has a very

clear observation (Camargo, Rodriguez, Côrtes, Aoki, Baladi, Arita, Watanabe, 2016). For this reasons of stability and rigidity, the digital processing of mandible CBCT images is selected to be studied in the thesis.

2.3.8 Trabecular bone texture features

Qualitative comparison of the considered Trabecular bone structure parameters as stated by physicians (McDonnell, McHugh, & O'Mahoney, 2007) for normal and osteoporotic are listed in Table 2.1.

Table 2.1: Comparison Between Normal and Osteoporotic Bone.

| Parameter | Normal | Osteoporotic |
|---------------------------------------|--------|--------------|
| Trabecular nodes (Tb.Nd); | High | Low |
| Trabecular termini (Tb.Tm) | Low | High |
| Trabecular separation (Tb.Sp) | Low | High |
| Trabecular spacing (Tb.Sc) | Low | High |
| Trabecular number (Tb.N) | High | Low |
| Trabecular thickness (Tb.Th) | High | Low |
| Bone volume over total volume (BV/TV) | High | Low |

2.3.9 Image Processing and Artificial Neural Networks

The image processing chain consists of the five different tasks as illustrated in Figure 4.2. Besides, optimizations techniques are used as a set of auxiliary tools that are available in all steps of the image processing chain (Petersen, Ridder, and Handels 2002).

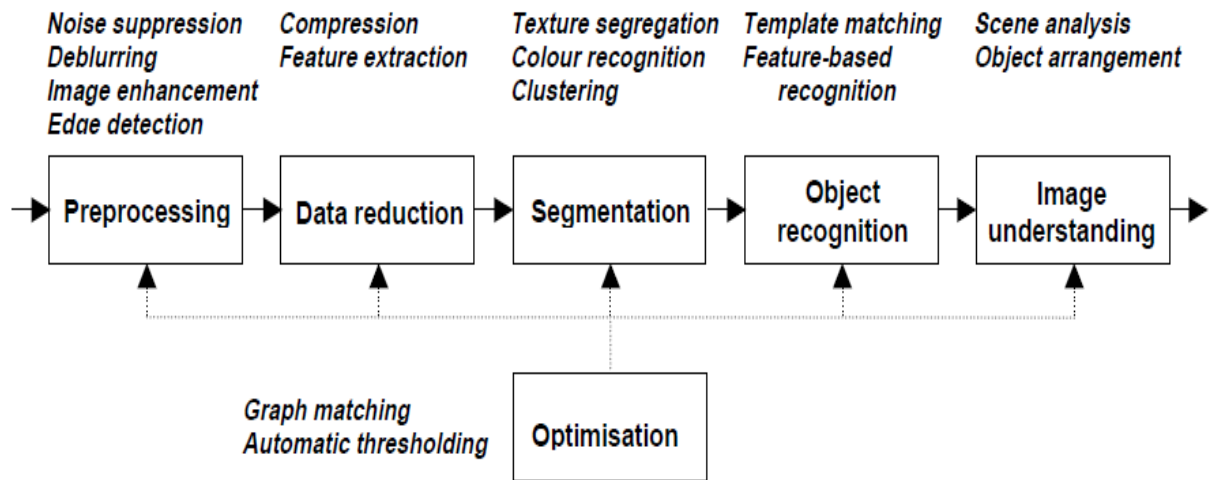


Figure 2.4: The Image Processing Chain (Petersen et.al. 2002).

NN's can be trained to perform the tasks in the image processing chain. NN can specify the type of task performed by the algorithm: preprocessing, data reduction, feature extraction, segmentation, object recognition, image understanding and optimization. Also can capture the abstraction level of the input data processed by the algorithm: pixel-level, local feature-level, structure level, object-level, object-set level and scene characterization. Each of the six types of tasks poses specific constraints to a neural-based approach. Segmentation or object recognition (Petersen et al. 2002).

2.3.10 Fundamental Steps in Image Processing:

(Tiwari, 2017), summarizes image processing steps as following in Figure 2.5:

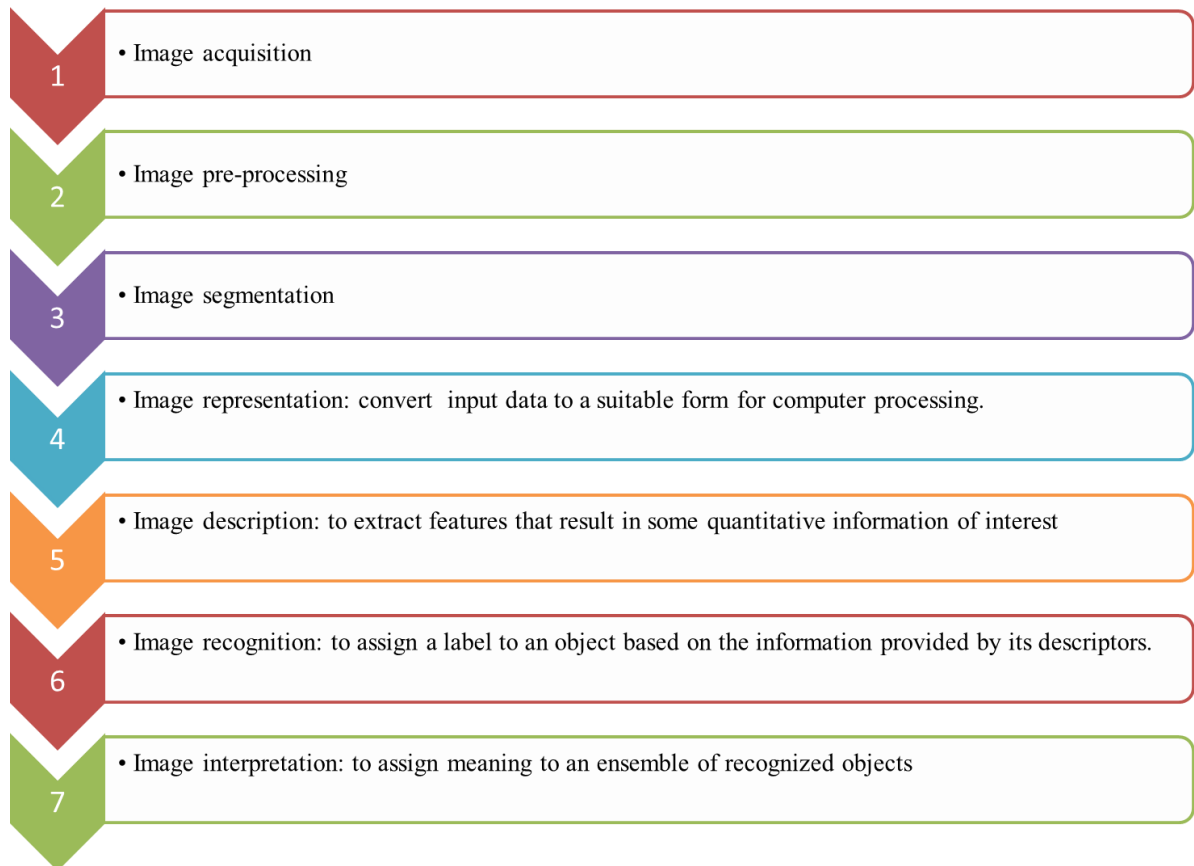


Figure 2.5 : Image Processing Steps.

2.3.10.1 Image Pre-processing

Image preprocessing is one of the preparatory steps which are highly required to ensure the high accuracy of the subsequent steps (Krig, 1993). preprocessing becomes necessary because most of the real life data is noisy, inconsistent and incomplete (Shameena & Jabbar, 2014). Preprocessing a bone image is a crucial initial step before texture analysis is performed.

2.3.10.2 Filtering

The filtering process involves getting rid of as much noise as possible while losing a minimum of information (Gedraite & Hadad, 2011) .

First, this section identifies noise, then it investigates the effects of a Gaussian blur on CBCT images.

- Noise

Medical images contain a large area of background noise (Gedraite et al. 2011). Noise is the unwanted pixels present in the image background that degrade the quality of the image (Yuvaraju & Haripriya, 2018). Noise can be represented as in equation 2.1

$$f(x, y) = g(x, y) + \eta(x, y) \dots \dots \dots (2.1)$$

Where $f(x, y)$ is the noisy image, $g(x, y)$ is the original image and $\eta(x, y)$ is the noise present in the image (Yuvaraju et al. 2018).

- Gaussian Filter

Noise can have a negative impact on the diagnosis. The filtering process involves reducing as much noise as possible while losing a minimum of information (Gedraite et. al., 2011).

Many studies have used the density correction using Gaussian blur introduced by White and Rudolph. However, most studies have used the same blurring parameters despite having different image resolutions (Hwang, Lee, Han, Kim, Jeong, Choi, & Park, 2017).

(Kulkarni & Bhavani k, 2018) analyzing the results of various works for segmentation of CT medical images, found that to get high accurate results the Gaussian filter is the best for reducing as much noise in DICOM images.

2.3.10.3 Binarization

The procedure to convert a gray scale image into a binary image is known as image binarization, Binary image could take only two values either 0 or 1 (Roy, 2013).

To convert to Binary image, the mathematical formula for this conversion is given below:

$$b(x, y) = 1 \text{ if } f(x, y) \geq T \text{ otherwise it is } 0 \dots\dots\dots(2.2).$$

While $f(x, y)$ is the input image. T is the threshold value, and $b(x, y)$ is the output image of the thresholding process (Shah, Haque, Islam, Ali, & Shabbir, 2010).

2.3.10.4 Segmentation

Image Segmentation is the process of partitioning a digital image into multiple regions or sets of pixels. Segmentation results are a set of regions that cover the entire image together and a set of contours extracted from the image (Muthukrishnan & Radha, 2011).

2.3.11 Edge Detection

The process of classifying and placing sharp discontinuities in an image is called the edge detection. They are basically used for feature detection and extraction (Rashmi, Kumar, & Saxena, 2013). Edge detection makes use of differential operators to detect changes in the gradients of the grey levels (Rashmi et al., 2013).

Mainly edge detection convolves the image through an operator that is defined to be perceptive to large gradients in the image and returning values of zero in identical regions.

The general criteria for edge detection include:

1. Detection should accurately catch as many edges shown in the image as possible, with lowest error rate.
2. Detection should accurately localize the edge point detected from the operator on the center of the edge.
3. The edge should only be marked once, and image noise should not create false edges where possible (Journal & Sciences, n.d.) .

2.3.11.1 Different Edge Detection Techniques

There is a very large amount of edge detection techniques available, each technique is designed to be perceptive to certain types of edges. Edge detection uses different operators to detect changes in the gradients of the grey levels. It is divided into two main categories illustrated in figure 2.6.

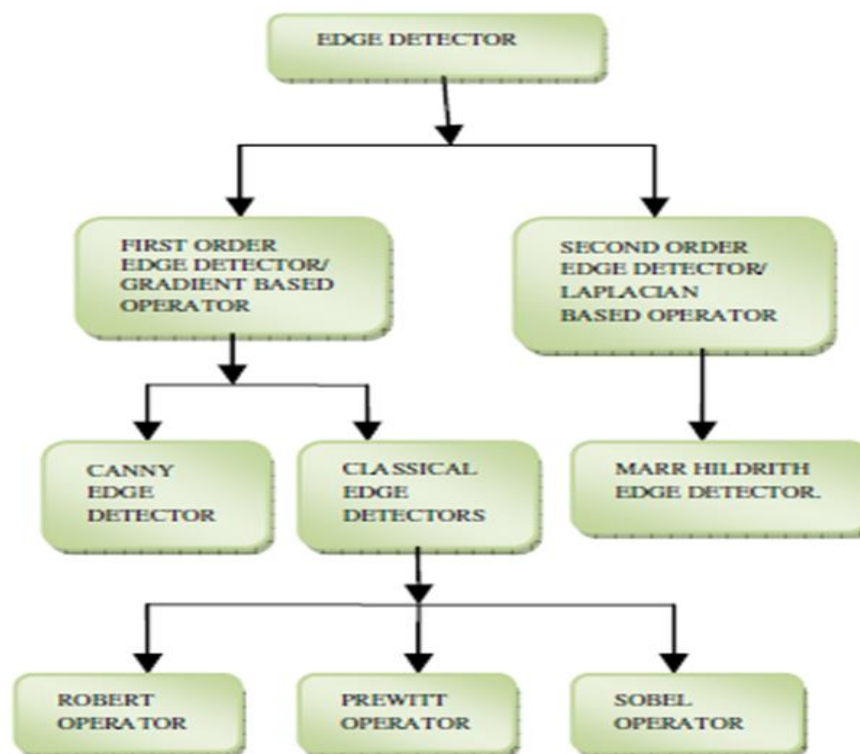


Figure 2.6: Types of Edge Detectors (Rashmi et al., 2013).

- **Marr-Hildreth or LoG edge detection**

The Laplacian of Gaussian (LoG) soothes the image and it computes the Laplacian, which produces a double edge image. Locating edges and finding the zero crossings between the double edges.

The Laplacian is generally used to find whether a pixel is on the dark or light side of an edge.

- **Roberts Edge Detection**

The Roberts edge detection is introduced by Lawrence Roberts (1965). It performs a simple, quick to compute, 2-D spatial gradient measurement on grayscale image. Every point Pixel value in the output represents the estimated complete magnitude of the spatial gradient of the input image at that point.

- **Sobel Edge Detection**

The Sobel edge detection method is introduced by Sobel in 1970. Sobel finds edges using the Sobel approximation to the derivative. It precedes the edges where the gradient is highest at those points. This method is used to find the estimated absolute gradient magnitude at each point in input grayscale image. The operator consists of a pair of 3x3 convolution kernels. One kernel is simply the other rotated by 90°. This is very similar to the Roberts Cross operator. Sobel edge detection has large kernel, as having larger mask.

- **Prewitt Edge Detection**

The Prewitt edge detection is proposed by Prewitt in 1970. Prewitt is a correct way to estimate the magnitude and orientation of an edge. Compared to Sobel operator Prewitt edge operator gives better performance.

- **Canny Edge Detection**

Canny edge detection technique is one of the standard edge detection techniques. It was first created by John Canny for his Master's thesis at MIT in 1983, and still outperforms many of the newer algorithms that have been developed. Canny's edge detector derives an "optimal" operator that minimizes the probability of multiply edge detection, minimized the probability of edge detecting failure and minimized the distance of the reported edge from the true edge (Ali & Clausi, 2002). Figure 2.7 shows the Block diagram of image enhancement (sharpening and de-noising) using canny edge detector.

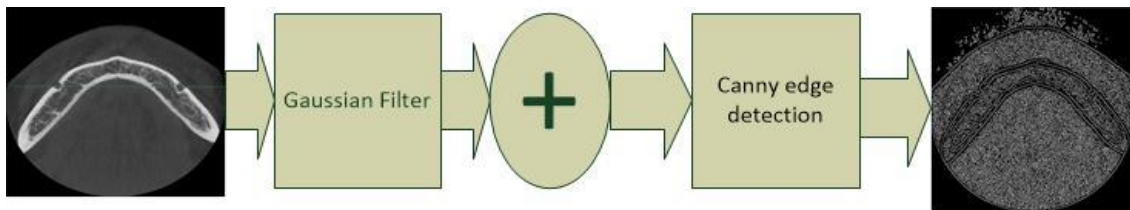


Figure 2.7: Block Diagram of Image Enhancement Using Canny Edge Detector

The algorithmic of canny edge detection technique steps are as follows:

- Convolve image with a Gaussian function to get smooth image.
- To compute edge strength, apply first difference gradient operator, then edge magnitude and direction are obtained.
- Apply non-maximal or critical suppression to the gradient magnitude.
- Apply threshold to the non-maximal suppression image.

2.3.12 Features Extraction

Feature extraction is one of the most important steps for recognizing osteoporosis from the mandible CBCT image. Trabecular bone texture feature is one of most important features. Using image analysis, image features which are dimensional with its component vector were extracted.

2.3.12.1 Texture Features Evaluation Techniques

Gueld, Keyzers, Deselaers, Leisten, Schubert, Ney and Lehmann (2004), presented an evaluation of methods for the automatic categorization of medical images. Categorization of medical images means image classification into a predefined order scheme. They evaluated and mentioned, global features describing color and shape such as: texture, structure, and down-scaled representations, those features being most suitable to distinguish medical images have been chosen.

1- Texture features proposed by Tamura

To describe an image's texture properties, Tamura suggested coarseness, contrast, and directionality, computed on a per-pixel basis.

Gueld et.al. Collected the values into a three-dimensional histogram ($6 * 8 * 8 = 384$ bins) and to measure the similarity between two histograms they used the Jensen-Shannon-divergence. All images were scaled into an identical size of $256*256$ pixels, ignoring the initial aspect ratio, to make the texture properties comparable.

2- Texture features proposed by Castelli

To describe image properties, Castelli et al, used various texture features. These encompass the global fractal dimension (computed using reticular cell counting), the coarseness, the gray-scale histogram entropy, some spatial gray-level statistics, and the circular Moran autocorrelation function. In all, 43 values are extracted from scaled images of fixed size ($256*256$ pixels).

3- Texture features proposed by Ngo

Ngo et al. used the variance of the first nine alternation current (AC) coefficients obtained by the discrete cosine transform (DCT) over all $8*8$ pixel blocks of an image. Results were improved when the direct current (DC) and some more of the AC coefficients are also considered. In this study, the first 21 DCT coefficients are used. The extraction was performed on identically sized images ($256*256$ pixels), when applied to medical images.

4- Image structure proposed by Zhou and Huang

Zhou and Huang proposed an algorithm to capture properties of edges within an image. A water-filling process is applied to the binarized gradient image. Canny's edge detector is used to determine the gradient.

The three parameters, the deviation of the Gaussian kernel used to smooth the image as well as the lower and the upper threshold for the edge tracing algorithm were empirically optimized. According to the authors' suggestion, Gueld et.al. Used the filling time, fork count, and loop count, both counts computed for a global and a per-edge-segment maximum. And the feature extraction was performed on images with 256*256 pixels.

2.3.12.2 Tamura Texture Based Extraction Method (Bagri & Johari, 2015)

Tamura proposed six different texture properties. Coarseness, Contrast, Directionality, Line-Likeness, Regularity and Roughness.

In most cases, the first three features are used because these features capture the high-level attributes of a texture and are also useful for browsing of images.

- **Coarseness**

Coarseness relates to the distance in gray levels of spatial variations, which is implicitly related to the size of primitive elements forming the texture (Bagri et. al., 2015). Coarseness was designed to measure differences between coarse and fine textures (Majtner & Svoboda, 2009).

An image will contain repeated textures pattern at different scales, coarseness aims to identify the largest size at which a texture exists, even where a smaller micro texture

exists. As shown in Figure 2.8, Fine textures have smaller value of this property than the coarse ones (Majtner et. al., 2009).

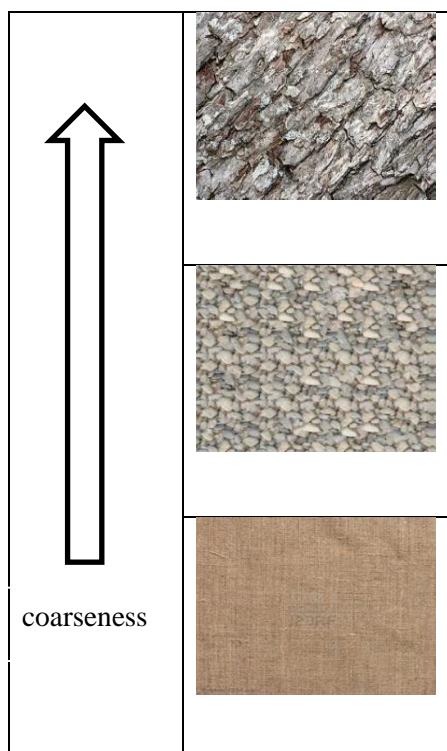


Figure 2.8: : Fine Textures Have Smaller Coarsness Value than the Coarse Ones.

To measure coarseness of an image, the following steps need to be applied:

1. Take the averages over the neighborhood, for each point (x, y) of the input image whose sizes are $2^e \times 2^e$, where $e \in \langle 0, \dots, 5 \rangle$:

$$A_l(x, y) = \frac{1}{2^{2l}} \sum_{i=x-2^{l-1}}^{x+2^{l-1}-1} \left(\sum_{j=y-2^{l-1}}^{y+2^{l-1}-1} f(x, y) \right) \dots \dots \dots (2.3)$$

2. Calculates the difference (E) between pair of averages corresponding to non-overlapping neighborhoods for each point on the opposite side of the point in horizontal and vertical direction.

Horizontal case:

$$E_{l,h} = |A_l(x + 2^{l-1}, y) - A_l(x - 2^{l-1}, y)| \dots \dots \dots (2.4)$$

Vertical case:

$$E_{l,v} = |A_l(x, y + 2^{l-1}) - A_l(x, y - 2^{l-1})| \dots \dots \dots (2.5)$$

3. At each point take the highest output value size. the coarseness will be the average of these values over the whole image for the image under consideration (Majtner et. al., 2009).

- **Contrast**

Contrast measures distribution of gray levels that varies in an image and to what extent its distribution is biased to black or white as shown in Figure 2.9.



Figure 2.9: Different Contrast

The second order and normalized fourth–order central moments of the gray levels are used to define the contrast.

To calculate contrast F_{con} the follows equation is used:

$$F_{con} = \frac{\sigma}{\sqrt[4]{\alpha_4}} \text{ with } \alpha_4 = \frac{\mu_4}{\sigma^4} \dots \dots \dots (2.6)$$

where μ_4 is the fourth moment about the mean μ , α_2 is the variance and the fourth root of α_4 to give the closest value according to tamura based on his experiment (Majtner et. al., 2009).

- **Directionality**

Directionality measures the frequency distribution of oriented local edges against their directional angle. Directionality measures the presence of orientation in the image not the orientation itself. If two images differs only in the orientation, the degree of this property will be the same for them (Majtner et.al. , 2009) as shown in Figure 2.10.



Figure 2.10:Two Images Differs in the Orientation (Majtner et.al. , 2009).

First we calculate the local edge direction for each point θ with the formula:

$$\theta = \tan^{-1} \frac{\Delta V}{\Delta H} + \frac{\pi}{2} \dots \dots \dots (2.7)$$

where ΔH and ΔV are horizontal and vertical derivatives respectively.

- **Line-Likeness**

In an image the average coincidence of direction of edges that co-occurred in the pairs of pixels separated by a distance along the edge direction in every pixel called Line-Likeness.

- **Regularity**

Measuring the regular pattern or similar that occurred in an image is called Regularity.

- **Roughness**

Summation of contrast and coarseness measures count Roughness.

2.3.12.3 Majtner et. al., (2009) suggestions of extending Tamura features for 3D images.

- **3D Tamura coarseness**

The 3D Tamura coarseness computation follows the same steps as in 2D case, but another dimension is added to the first step, for each point (x, y, z) , as in equation 2.8.

$$A_l(x, y, z) = \frac{1}{2^{3l}} \sum_{i=x-m}^{x+m-1} \left(\sum_{j=y-m}^{y+m-1} f(x, y, z) \right) \dots \dots \dots (2.8)$$

Where $m = 2^{e-1}$ and e determines the size of neighborhood, that is $2^l \times 2^l \times 2^l$. In 2D case.

This part of the algorithm depends on the size of particular images. In the second step of computing 3D Tamura coarseness, take the differences by the same way as in 2D case but for three directions instead of two, calculated by the equations 2.9, 2.10, and 2.11 for the x-axis, y-axis, and z-axis, respectively.

$$E_{l,h} = |A_l(x + 2^{l-1}, y, z) - A_l(x - 2^{l-1}, y, z)| \dots \dots \dots (2.9)$$

$$E_{l,v} = |A_l(x, y + 2^{l-1}, z) - A_l(x, y - 2^{l-1}, z)| \dots \dots \dots (2.10)$$

$$E_{l,z} = |A_l(x, y, z + 2^{l-1}) - A_l(x, y, z - 2^{l-1})| \dots \dots \dots (2.11)$$

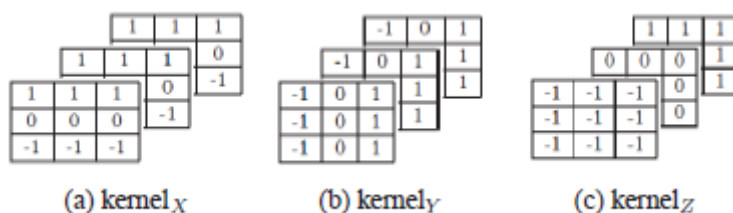
- **3D Tamura contrast**

The algorithm for contrast is applicable on images of any dimensionality, and the only one feature from Tamura's set that can be derived from the 2D case by simply adding another dimension in the original method. Tamura contrast in 3D is used in the same way as it was presented for 2D case.

• **3D Tamura directionality**

3D Tamura Directionality cannot be derived from 2D case straight forwardly.

First, need to form convolution kernels to compute derivation in three directions along three axes.



Then use these kernels to create derivatives in x-axis (ΔX), y-axis (ΔY) and z-axis (ΔZ) by convolution with input image. Then calculate the following formulas:

$$\theta_1 = \tan^{-1} \frac{\Delta Y}{\Delta X} + \frac{\pi}{2} \dots \dots \dots (2.12)$$

$$\theta_2 = \tan^{-1} \frac{\Delta Z}{\Delta Y} + \frac{\pi}{2} \dots \dots \dots (3.13)$$

$$\theta_3 = \tan^{-1} \frac{\Delta X}{\Delta Z} + \frac{\pi}{2} \dots \dots \dots (3.14)$$

Then create 16 bin histogram each of n values, where $n \in \{1, 2, 3\}$. Then get the final result in the same way as in 2D case. (Majtner et. al. , 2009).

2.3.13 Classification

Classification is defined as categorizing images into groups or classes based on their extracted features vector.

2.3.13.1 The Back-Propagation Classifier

The Back-Propagation neural network is a kind of Artificial Neural Network, with learning's algorithm based on the Deepest-Descent technique. It has the ability to minimize the error of nonlinear functions of high complexity, if provided with a suitable number of Hidden units (Buscema, Massimo.1998).

- **Activation Function**

Activation function f is a mathematical operation used by the neurons to decide its output signal. It is usually chosen depending on the type of problem to be solved by the network. Figure 18 illustrates the activation function in the proposed BP-ANN. It is a sigmoid signal, which is a non-linear curved S-shaped function as shown in Figure 2.11. This function is the most commonly used of activation function. Sigmoid function is strictly increasing function by nature (Panchal & Panchal, 2014).

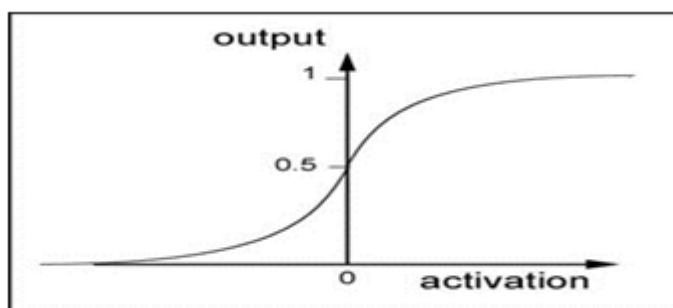


Figure 2.11: Sigmoidal Function.

2.4 Related Work

This section presents a number of related works in order to determine the major research techniques and methodologies to be used in the course of this thesis.

Shi & He., (2010) described the major strengths and weakness of applying neural networks for medical image processing.

Shi et al. found that it does not matter what model of NN used for treated medical image, compared to traditional image processing methods, and time to apply trainers neural network for medical image processing solution the problem was very small, although training the NN is the cost of working time as well as medical image processing tasks often require very complicated account .

Despite their success story in the medical picture treatment, ANN's have several key disadvantages the first is that the neural network is difficult to express knowledge and experience of the human expert, and building its topological structure lacks theoretical methods, the material meaning of its common weight is unclear.

The second problem relates to the amount of input data. To achieve high and reliable performance Lack of training, and a large number of training cases usually required. If ANN is trained with only a few cases, the circular capacity will be lower. Because medical images are progressing rapidly like the technology advances.

Koh et al., (2011) evaluated the potential use of the computed tomography indices (CTI) on CBCT images for an assessment of the bone mineral density (BMD) in osteoporotic women. Twenty-one osteoporotic women and 21 healthy women were enrolled as the subjects. The BMD of the lumbar vertebrae and femur were calculated by DEXA using a DEXA scanner. The CBCT images were obtained from the unilateral mental foramen region using a PSR-9000NTM Dental CT system. The axial, sagittal, and coronal images were reconstructed from the block images using on demend3DTM.

The relationship between the CT measurements and BMDs were assessed and determined.

Koh et al., (2011) concluded that there were significant differences between the normal and osteoporosis groups in the CTI(S) and CTI (I). On the other hand, there was no correlation between the groups in the CTMI.

Barnkgei et. al., (2014) aimed to evaluate the use of dental (CBCT) in the diagnosis of osteoporosis using only a CBCT viewer program.

Thirty-eight women who underwent dual-energy X-ray absorptiometry (DEXA) examination for hip and lumbar vertebrae were scanned using CBCT (field of view: 13 cm×15 cm; voxel size: 0.25 mm). Slices from the body of the mandible as well as the ramus were selected and some CBCT derived variables, such as radiographic density (RD) as gray values, were calculated as gray values. Pearson's correlation, one-way analysis of variance (ANOVA), and accuracy (sensitivity and specificity) evaluation based on linear and logistic regression were performed to choose the variable that best correlated with the lumbar and femoral neck T-scores. They found that RD of the whole bone area of the mandible was the variable that best correlated with and predicted both the femoral neck and the lumbar vertebrae T-scores.

Barnkgei et al., (2015), Predicted osteoporosis based on the cervical vertebrae CBCT-derived radiographic density (RD) using the CBCT-viewer program for 38 women. The RD as gray values for the first and second vertebrae, and the density was calculated by using CBCT-viewer software (White Fox imaging) as shown in Figure 2.12. The right and left parts of the first and the second vertebrae with its odontoid process (dens) appear in this slide. B, Adjusting the window width and level to 0 and 400 gray values, respectively. C, calculating the radiographic density (RD) of the left and right parts of the first and the second vertebrae D.

Strongest correlation coefficients accuracy (90.8%, 86.4%) in predicting osteoporosis in the lumbar vertebrae and the femoral neck, respectively are reported. This finding should be confirmed on other CBCT devices, and the cervical vertebrae rarely appear in CBCT for dental matters.

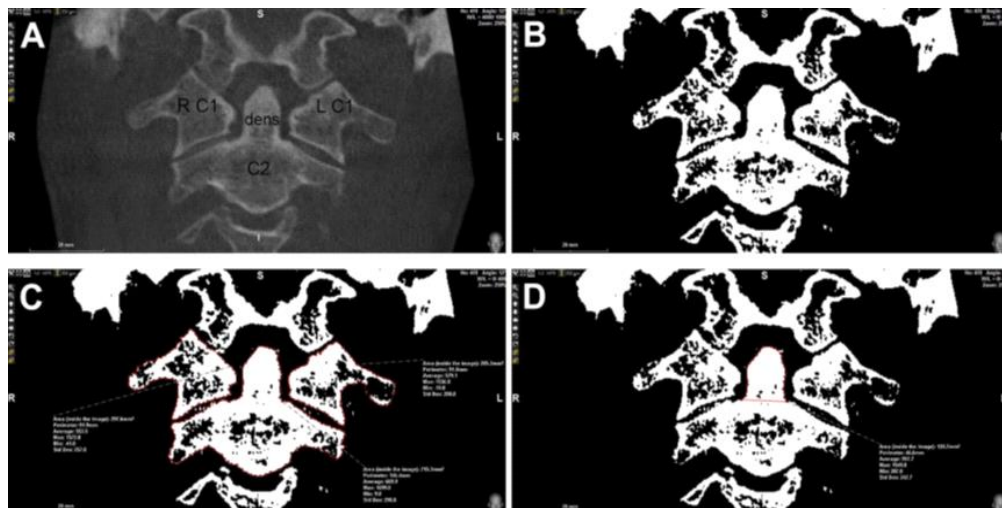


Figure 2.12: The Selected Coronal Slice After Angulation Adjustment of CBCT Image.

Kannan et al., (2015) used the evaluation of alveolar bone changes and thus serve as a valuable predictor for osteoporosis.

Totally 91 women above 50 years of age were included in this study. CBCT used was ORTHOPHOS 3D, Sirona (Germany) at 90 Kv. MCI, MCT, MI and bone loss was assessed from the radiograph.

They explained that there was no significant relationship in mental index between right and left side at the mental foramen region. There was a statistical significance between mental index and Mandibular cortical index which was done using one-way ANOVA (0.019). In this method the density of bone is considered as an important factor.

Further studies with larger samples will be helpful to establish a significant relationship between radio morphometric indices and osteoporosis. Future studies compared with gold standard dual energy X-ray absorptiometry (DEXA) can be done to standardize the correlation of radio morphometric indices and osteoporosis.

Badamia, (2015) paper is a review of the use of NN's in Medical Imaging Process, with its historical background. and an explanation why it has become so important in modern medical image processing, a biological and artificial neuron is then compared and

the working in pattern recognition, advantages of ANN over conventional computer programs, types of neural networks, an introduction of the application in the medical image processing, and various forms of algorithms for different image analysis and their advantages.

The papers conclude with an emphasis that ANN has not only improved medical image processing, it is likely to take a leading role in medication in the coming years.

Beatriz et. al., (2016) proposed a technique aimed to evaluate the validity of cone-beam computed tomography (CBCT) for assessing mandibular bone quality using the Klemetti classification. He used panoramic radiography (PAN) The most commonly studied qualitative measure of mandibular morphology in relation to osteoporosis. Erosions of the inferior border are typically scored using the mandibular cortical index. This index (known as the Klemetti index). 30 women between the ages of 45 and 80 years were evaluated based on the Klemetti classification in panoramic radiographs used as reference images. Afterwards, panoramic reconstruction and cross-sectional slices of CBCT examinations of these patients were analyzed and categorized according to the same classification.

No differences were found between the diagnostic results based on panoramic radiography and panoramic reconstruction. And the results were statistically different from the others.

Based on the disagreement found between the panoramic radiographs and the CBCT cross-sectional slices, the Klemetti classification is not an adequate means of assessing bone quality with CBCT.

Güngör et. al., (2016) Performed DEXA on 90 patients aged over 30 years who underwent CBCT, included 26 osteoporosis patients, 33 osteopenia patients and 31 were

healthy. CBCT images were obtained with i-CAT, using a 130×100 mm field of view (FOV). The nominal beam was 120 kV and 18.59 mA, with 8.9 sec rotation time, and a voxel size of 0.3 mm. CBCT images of jaw bones were evaluated using radio morphometric indexes, CT values, histogram analysis (HA) and fractal dimension (FD) analysis. Right and left mandibular radio morphometric indexes, CT values and HA measurements in osteoporosis patients were significantly lower than measurements in osteopenia patients and control subjects.

Positive correlations were observed between measurements of spine bone mineral density (BMD) and right and left mandibular CT values and HU measurements. Left maxilla FD measurements in osteoporosis patients were significantly lower than in the control and osteopenia. The study didn't conclude an accurate unique value to detect osteoporosis.

Suprijanto & Azhari et al., (2016) reported a scheme that consists of the determination of the ROI the condyle mandibular in the image as biomarker and feature extraction from ROI and classification of bone conditions. For feature extraction, the fraction of intensity values in the ROI that represent high bone density and the ROI total area is performed. The classification evaluated from the ability of each feature and its combinations for the BMD detection in two classes (normal and abnormal), with the ANN method. The evaluation system used 105 panoramic image data which consist of 36 training data and 69 test data that were divided into two classes.

The two classes of classification obtained 88.0% accuracy rate and 88.0% sensitivity rate.

Esmaeli et al., (2017) provided CBCT images of 108 patients by using NewTom VGI (QR, Verona, Italy), in FoV (15×12 cm²) at amorphous silicon flat panel detector,

voxel size of 0.2 mm, and focal spot size of 0.3 mm. This system uses rotating anode: 110 kV and 1–20 mA, and takes images at 360 rotations and the scan time is 18 sec. All the exposure parameters were set automatically). Then the patients were assigned to osteoporosis, osteopenia and healthy group, using the T-score derived from the DEXA technique. These images were observed by NNT Viewer software on a 19-inch Phi-lips 190B LCD (Philips, Eindhoven, Netherland) with a resolution of 1024×1024 and 16 bit in a room with a dim light and without any windows. In order to show that there was no difference in the RD measurement between different scans, the homogeneity of RD was tested between scans by using distilled water and this procedure was repeated during the scanning of all the patients. According to the device's bit depth, differences in RD rate of water .These steps lead to the creation of a homogenous density between different scans and enhancement of credibility of the present study. Finally, RD of the lateral mass was measured. RD values were compared between the three groups, the first and second cervical vertebrae in the three groups showed that all the values had statistically significant differences.

Based on the findings of this study, it is possible to predict the osteoporosis status of the patient through the RD related to the body of C2 and the left lateral mass of C1 more accurately than the other areas.

The techniques in this study are strictly and hard to implement also the study didn't conclude an accurate unique value to detect osteoporosis.

Alkhader et. al., (2018) evaluated the usefulness of measuring bone density of mandibular condyle (BDMC) in patients at risk of osteoporosis. Two hundred and four mandibular condyles (46 condyles from males and 158 condyles from females) were examined by CBCT. Using Vivo software, BDMC and mental index (MI) were measured

by two observers and correlated using Pearson's correlation coefficients. Patients were divided into high risk and low risk of osteoporosis using 3.1 mm of MI as a cutoff value, and the mean value of BDMC was compared and correlated using independent samples t-test and regression analysis.

The mean value of BDMC was moderately correlated with MI, and in female patients at low risk of osteoporosis, the mean value of BDMC was significantly higher than in patients at high risk of osteoporosis.

After reviewing previous studies that are related to the research methodology, a comparison between these studies are conducted as given in Table 2.2.

Table 2.2: Comparison Between related work.

| Author & year | Implementation | Conclusion |
|--------------------|-------------------------------------------------------------------------------------------------------------------------------------------------------------------------------------------------------------------------------------------------------------------------------------|---------------------------------------------------------------------------------------------------------------------------------------------------------------------------------------------------------------------------------------------------------------------------------------------|
| Shi & He., (2010) | Described strengths and weakness of applying ANN for medical image processing. | Found that it does not matter what model of NN used for treated medical image, compared to traditional image processing methods. If ANN is trained with only a few cases, the circular capacity will be lower. Because medical images are progressing rapidly like the technology advances. |
| Koh et al., (2011) | Evaluated the potential use of the (CTI) on CBCT images for an assessment BMD in osteoporotic women. The CBCT images were obtained from the unilateral mental foramen region, The axial, sagittal, and coronal images. The relationship between the CT measurements and BMDs | There were significant differences between the normal and osteoporosis groups in the CTI(S) and CTI (I). On the other hand, there was no correlation between the groups in the CTMI. |

| | | |
|--------------------------|-----------------------------------------------------------------------------------------------------------------------------------------------------------------------------------------------------------------------------------------|-----------------------------------------------------------------------------------------------------------------------------------------------------------------------------------------------------------|
| | were assessed and determined. | |
| Barnkggei et al., (2014) | Evaluated the use of dental CBCT in the diagnosis of osteoporosis using only a CBCT viewer program. Slices from the body of the mandible as well as the ramus were selected and some CBCT derived variables, such as RD as gray values. | RD of the whole bone area of the mandible was the variable that best correlated with and predicted both the femoral neck and the lumbar vertebrae T-scores. |
| Barnkggei et al., (2015) | Predicted osteoporosis based on the cervical vertebrae CBCT-derived RD using the CBCT-viewer program. RD as gray values for the first and second vertebrae, and the density was calculated by using CBCT-viewer software | Strongest correlation coefficients accuracy (90.8%, 86.4%) in predicting osteoporosis in the lumbar vertebrae and the femoral neck, respectively. This finding should be confirmed on other CBCT devices. |
| Kannan et al., (2015) | Used the evaluation of alveolar bone changes and thus serve as a valuable predictor for osteoporosis. | There was no significant relationship in mental index between right and left side at the mental foramen region. There |

| | | |
|-------------------------|---------------------------------------------------------------------------------------------------------------------------------------------------|----------------------------------------------------------------------------------------------------------------------------------------------------------------------------------------------------------------------------------------------------------------------------------------------------------------------------------|
| | MCI, MCT, MI and bone loss was assessed from the radiograph. | was a statistical significance between mental index and Mandibular cortical index. |
| Badamia, (2015) | Paper is a review of the use of NN's in Medical Imaging Process. With its historical background | ANN has not only improved medical image processing, it is likely to take a leading role in medication in the coming years. |
| Beatriz et. al., (2016) | Evaluated the validity of CBCT for assessing mandibular bone quality using the Klemetti classification. | The Klemetti classification is not an adequate means of assessing bone quality with CBCT. |
| Güngör et. al., (2016) | CBCT images of jaw bones were evaluated using radio morphometric indexes, CT values, histogram analysis (HA) and fractal dimension (FD) analysis. | Positive correlations were observed between measurements of spine BMD and right and left mandibular CT values and HU measurements. Left maxilla FD measurements in osteoporosis patients were significantly lower than in the control and osteopenia. The study didn't conclude an accurate unique value to detect osteoporosis. |

| | | |
|-----------------------------------------------|----------------------------------------------------------------------------------------------------------------------------------------------------------------------------------------------------------------------------------------------------------------------------------------------------------------------------------------------------------------------------------------------------------------------------------------------------|-----------------------------------------------------------------------------------------------------------------------------------------------------------------------------------------------------------------------------------|
| <p>Suprijanto & Azhari et al., (2016)</p> | <p>Determined the RoI the condyle mandibular as biomarker and feature extraction from RoI and classification of bone conditions. For feature extraction, the fraction of intensity values in the RoI that represent high bone density and the RoI total area is performed. The classification evaluated from the ability of each feature and its combinations for the BMD detection in two classes (normal and abnormal), with the ANN method.</p> | <p>The two classes of classification obtained 88.0% accuracy rate and 88.0% sensitivity rate.</p> |
| <p>Esmaeli et al., (2017)</p> | <p>The first and second cervical vertebrae RD values were compared between three groups, osteoporosis, osteopenia and healthy groups.</p> | <p>It is possible to predict the osteoporosis through the RD related to the body of C2 and the left lateral mass of C1 more accurately than the other areas. The techniques are strictly and hard to implement also the study</p> |

| | | |
|--------------------------|-----------------------------------------------------------------------------------------------------------------------------------------------------------------------------------------------------------------------------------------|--------------------------------------------------------------------------------------------------------------------------------------------------------------------------------------------------------------|
| | | didn't conclude an accurate unique value to detect osteoporosis. |
| Alkhader et. al., (2018) | Evaluated the usefulness of measuring bone density of mandibular condyle (BDMC) in patients at risk of osteoporosis. BDMC and mental index (MI) were measured by two observers and correlated using Pearson's correlation coefficients. | The mean value of BDMC was moderately correlated with MI, and in female patients at low risk of osteoporosis, the mean value of BDMC was significantly higher than in patients at high risk of osteoporosis. |

2.5 Summery

In this chapter, several studies that are related to osteoporosis detection were reviewed, described, analyzed, and summarized. Each of the discussed literature in this chapter achieved a certain goal, but did not conclude an accurate value to surely detect osteoporosis from mandible CBCT without the need for the DEXA scan.

This study is intended to design and implement image analysis and AI algorithms in order to specify features value in CBCT with the main purpose of detecting osteoporosis.

CHAPTER 3

Methodology and the Proposed Technique

Chapter Three

Methodology and the Proposed Technique

3.1 Overview

This chapter presents the proposed methodology. The chapter is organized as follows: Section 3.2 is an introduction about the chapter. Section 3.3 lists the materials used for this study. Section 3.4 presents and analyzes the proposed algorithm to create a features vector; Section 3.5 shows the proposed BP-ANN classifier that outlines the features vector used as input to classify the CBCT image as normal or osteoporotic. Finally, Section 3.6 gives a summary of this chapter.

3.2 Introduction

The golden standard of measurement for bone mass density, BMD or the aspects that is related to bone structure is DEXA (Esmaeli et al., 2017). This work will report an alternative way, that contains the determination of the RoI in the image and feature extraction from RoI and classification of bone conditions.

RoI will be taken from the mandibular area. The classification will be evaluated from the ability of the features and their combination for the bone structure detection in two classes, normal and abnormal, implementing artificial neural network classifier.

3.3 Materials

Ethical clearance for this study was obtained from Department of Dentomaxillofacial Radiology, Dentistry Faculty, Jordan University Hospital, Amman, Jordan. The research samples that will be obtained from patients' data consist of CBCT

and BMD information that was already determined by DEXA and the diagnosis is already been done by specialized physician. The data under consideration will acquire age range of 50-85 years old women.

The patients CBCT images will be assigned into two groups; osteoporosis and healthy (normal), using the T-score derives from the DEXA technique.

Everest Digital Radiology Center provided us with CBCT images of patients using CS8100 3D carestream health Inc. machine. This system uses rotating anode: 75 kvp and 4 mAs.

3.4 Methodology and Design

The diagnosis algorithm proposed in this paper is designed for automatic detection of Osteoporosis in CBCT images. The system consists of four modules: (i) Image Preprocessing, (ii) Segmentation of trabecular bone, (iii) Extraction of segmented image features, and (iv) Recognition using artificial neural network classifier. Figure 3.1 illustrates the block diagram for the overall system architecture.

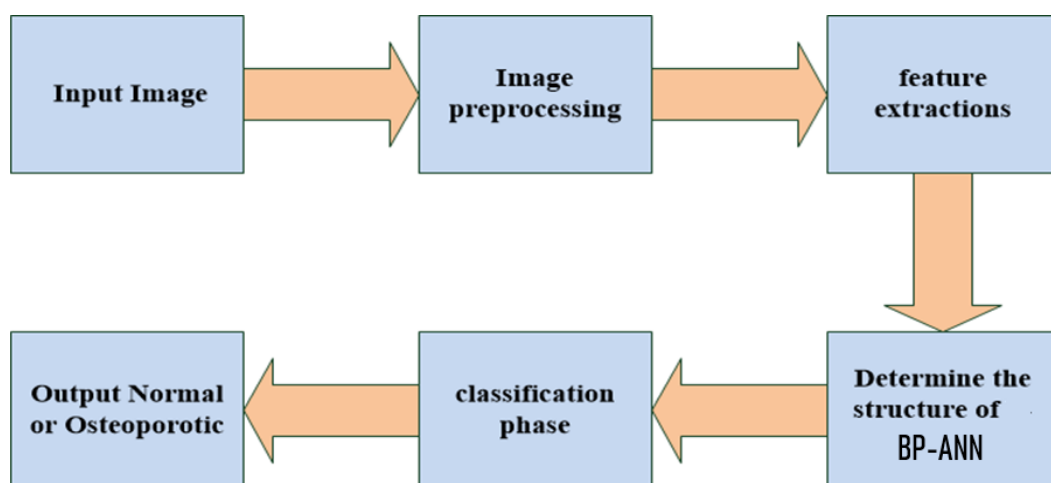


Figure 3.1: Proposed System

3.4.1 Image Processing

This module aims to process and analyze CBCT images, so that high quality information can be produced for osteoporosis prediction.

3.4.1.1 Input Image

Image acquisition is the process of obtaining the mandible slice where both foramina appear simultaneously on the coronal views (the green line). This is checked by navigating through all the CBCT image slices. An image sample is shown in Figure 3.2.



Figure 3.2: Mandible Slice Where Both Foramina Appear Simultaneously.

3.4.1.2 Image Pre-processing

Dicom image passed through the preprocessing steps. Preprocessing includes noise removal and the elimination of redundant information as far as possible. Figure 3.3 shows the block diagram of image pre-processing steps. This following sub-section describes each steps of image pre-processing as follows.

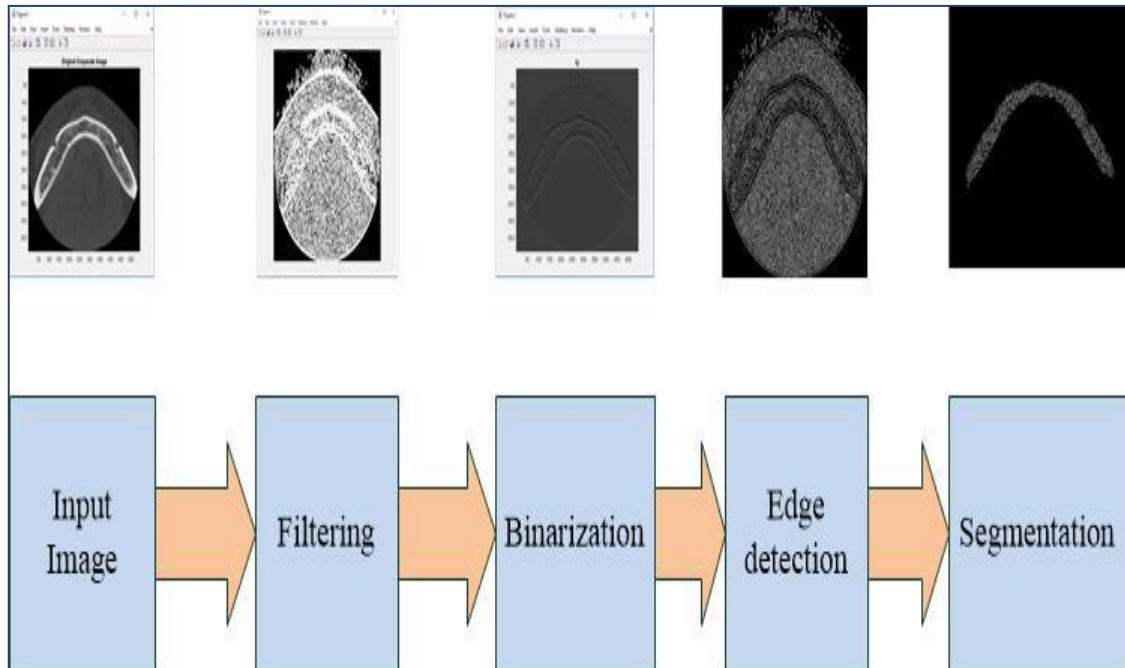


Figure 3.3: Block Diagram of Image Pre-processing Steps.

- **Filtering Using Gaussian Filter**

The noisy image $f(x, y)$ convolves with a Gaussian function in order to get smooth image $f'(x, y)$ as in equation 3.1.

$$F'(x, y) = f(x, y) * G(x, y, \sigma) \dots\dots\dots(3.1)$$

Where σ is the standard deviation of the distribution (Muthukrishnan et al. 2011).

- **Binarization**

Threshold value is determined by analyzing the histogram of the grayscale image, and then it is defined, such that pixel values equal or over threshold are set as one, and for pixels with values under this threshold as zero. The ones represent white and zeros represent black.

- **Edge Detection**

It is found experimentally, that Canny edge detection technique with threshold produces the most accurately edge detection from CBCT image.

Figure 3.4 shows the flow chart of canny edge detection algorithm.

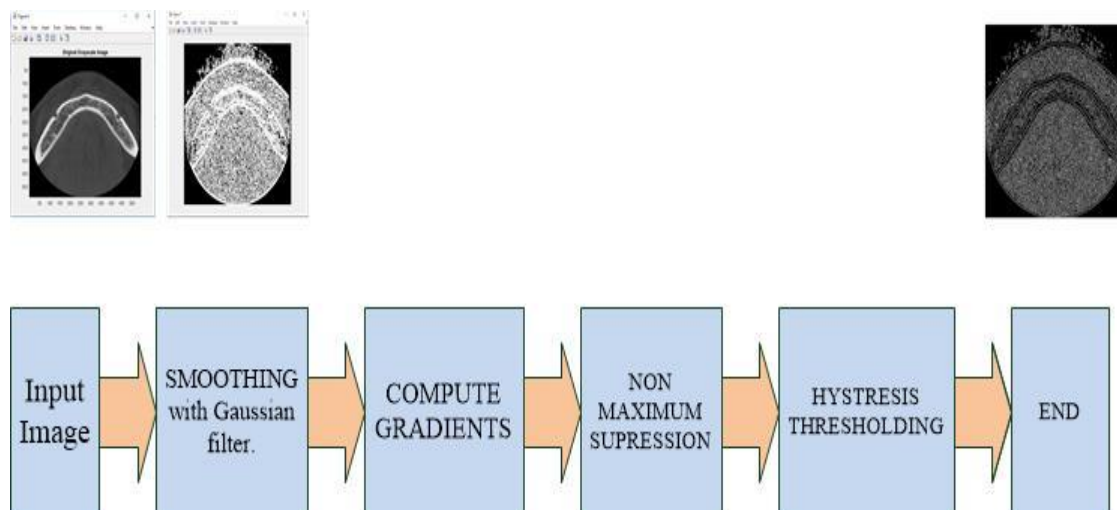


Figure 3.4: Flow Chart of Canny Edge Detection Algorithm.

Pseudocode below summarize the steps used to apply canny edge detection for image

Input: 3D-grayscale image contains n points, represented by p ($p_1, p_2, p_3, \dots, p_n$), Where each cell has p_i (p_{1x}, p_{1y}, p_{1z})^t, Where p_{1x} denotes the average point in that cell in x direction.

Output: Canny edge detecting image $C(x,y,z)$

Steps: For each cell:

- Filtering phase: using Gaussian Filter
- compute Gradient
- Calculate non- maximal suppression $C(x,y,z)$
- Threshold $C(x,y,z)$

END

Segmentation

CBCT image slice will be digitally segmenting to extract the inner trabecular bone, where only the region of interest for the test is left.

3.4.2 Feature Extraction

Trabecular bone texture features are the most important one to be considered here. For the solution to this specific problem, this study adopted the best well known method, namely Tamura texture features extraction-based method modified by adding four more important features by the author which are the number of non-zero matrix elements, length of edges, number of edges, and average of one edge length.

Coarseness, contrast, direction, number of non-zero matrix elements, length of edges, number of edges, and average of one edge length, are good indicators to the bone parameter mentioned above.

- If the bone has a low Tb.Nd, Tb.N, Tb.Th, and BV/TV and high Tb.Tm , Tb.Sp and Tb.Sc then coarseness, contrast, direction, and mean edge length will be high. And the number of non-zero Pixels, length of edges and number of edges will be low.
- If the bone has a high Tb.Nd, Tb.N, Tb.Th, and BV/TV and high Tb.Tm , Tb.Sp and Tb.Sc then coarseness, contrast, direction, and mean edge length will be low. And the number of non-zero Pixels, length of edges and number of edges will be high. The features that will be extracted from mandible CBCT images are listed in Table 3.1.

Table 3.1:Criteria of the Used Dataset Variables as Input.

| Input | Parameter | Osteoporotic | healthy |
|--------------|------------------------------------|---------------------|----------------|
| P1 | Coarseness | High | Low |
| P2 | Contrast | High | Low |
| P3 | Direction | High | Low |
| P4 | Average of Edge Length | High | Low |
| P5 | Length of Edges | Low | High |
| P6 | Number of Edges | Low | High |
| P7 | Number of Non-zero Matrix Elements | Low | High |

A modified Tamura texture-based extraction method will be used to look for the important trabecular bone texture features that can assist in the investigation for the Tamura Features in 3D.

3.4.3 Classification

A back-propagation neural network was created in order to perform the classification for the images under consideration, as in the following.

3.4.3.1 The Proposed Diagnosis Model

A feed-forward back propagation artificial neural network (BP-ANN) is proposed to perform the classification for the diagnosis of osteoporosis (Angus, 1991). The BP-ANN is built using MATLAB 2018b. It consists of three layers; an input layer, a hidden layer, and an output layer. The number of input layer nodes is equal to the selected parameters to be used (which are seven features in this experiment). Although more than one hidden layer may be used, it is found that one hidden layer with 15 hidden layer

neurons was satisfactory. And the output layer consists of one neuron that will produce the class of the patient whether suffering osteoporosis or being normal.

The data to be used in this experiment is the calculated values of the selected features from the CBCT images together with its corresponding patient's status and will be used as the input parameters. These parameters will be randomly chosen and automatically divided into two groups, 60% will be used as training set for the BP-ANN experimentation and the remaining 40% will be used the validation and test sets. A sigmoid signal is selected as activation function for the network.

The input layer number of neurons is determined by the number of features selected, which is seven in this experiment and the number of neurons for the output layer is determined by the number of expected target classes, which is only one for the proposed classification network. And the number of neurons in the hidden layer is determined based Hecht-Nielsen theorem, which states that any continuous function can be represented by a neural network that has only one hidden layer with exactly $(2n + 1)$ nodes, where n is the number of input nodes (Hecht-Nielsen 1987), hence, it is chosen to be 15 hidden neurons. Figure 3.5 depicts the illustration for the BP-ANN, adopted in this research work.

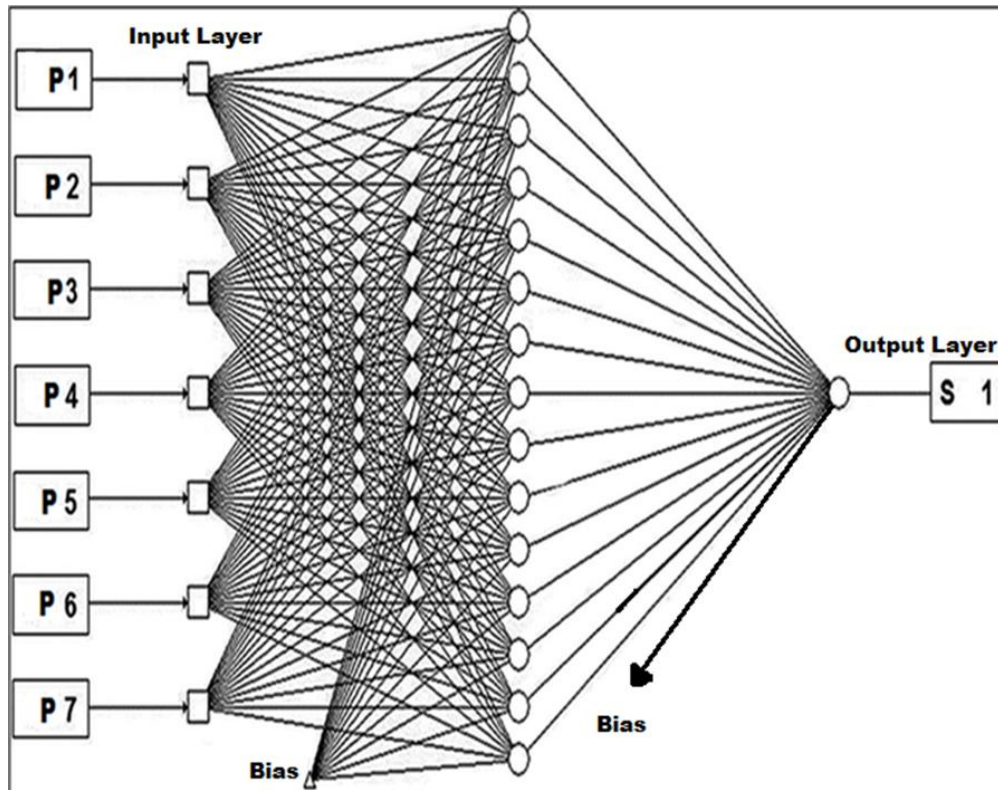


Figure 3.5: Architecture of NN (7:15:1).

• Learning Methods of B-PANN

Supervised learning a teacher is present during learning process. In this process, the expected output is already presented to the network. The data to be used as training set consists of values for the seven parameters with their corresponding output values.

The training will start by setting all the weights to initial values of zero, and then the network will iterate for as many times as required to converge to the classification required.

Experimenting on various values for the Learning rate (α) or the training factor, it is found that $\alpha = 0.01$ gives the fastest convergence for this network. The convergence was achieved after 35 iterations. Table 3.2, lists a summary of all the components and

parameters for proposed BP-ANN. It must be mentioned here too, that the cross entropy was adopted as the measurement criteria.

Table 3.2: The Architecture and Parameters of the Designed NN.

| Architecture | |
|--------------------------------------|------------------|
| Number of input neurons, n | 7 |
| Number of hidden layers | 1 |
| Number of neurons in hidden layer, m | 15 |
| Number of output layer neurons, | 1 |
| Activation function | Sigmoid |
| Learning method (rule) | Back-Propagation |
| Learning rate, α | 0.01 |
| Number of iterations (epochs) | 35 |
| Measurements | Cross-Entropy |

Once feature vectors were extracted for every slice in RoI, the goal was then to use them in a machine learning task to predict their label as osteoporotic or non- osteoporotic in each case.

3.4.4 Training Phase

A training phase consists of five major steps in the proposed BP-ANN classifier, they are illustrated in Figure. 3.6.

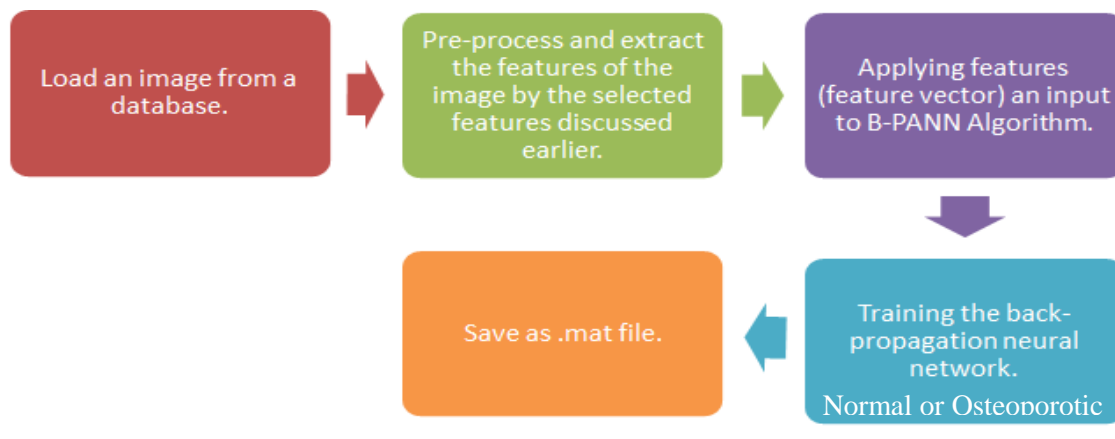


Figure 3.6: Training the Back- Propagation Neural Network.

3.4.5 Testing Phase

The testing stage in the proposed BP-ANN classifier consists of five major steps that are illustrated in Figure 3.7.

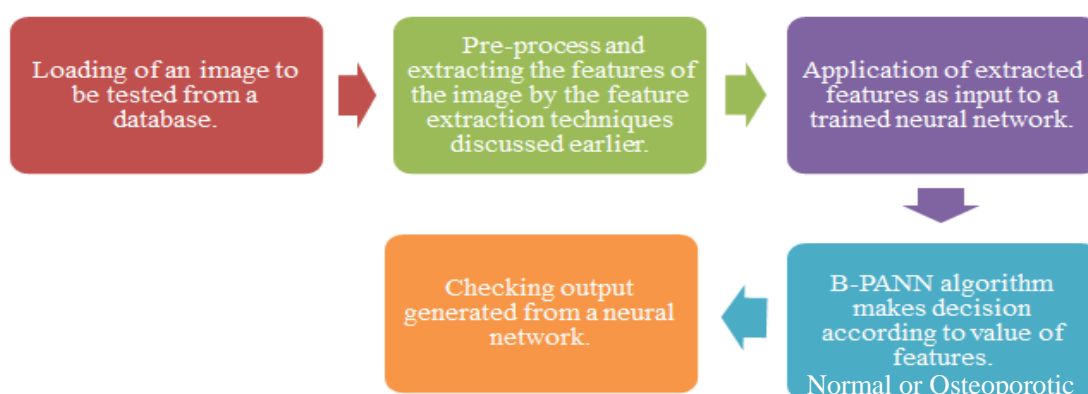



Figure 3.7: Testing Phase Steps.

3.5 Summary

In this chapter, the system proposed a design for automatic detection of osteoporosis using CBCT images by analyzing pattern of bone loss in trabecular mandible bone to extract a features vector that will be used as inputs in a machine learning task to predict their label as osteoporotic or non-osteoporotic in each case.



CHAPTER 4

DESIGN, IMPLEMENTATION,
AND TESTING

Chapter Four

Design, Implementation, and Testing

4.1 Overview

This chapter is about the image processing techniques that are used to prepare an image to extract features vector that will be used as an input to BP-ANN classifier to detect osteoporosis. It is organized as follows: Section 4.2 is an introduction to the experiment. Section 4.3 shows the details of the datasets that are used. Section 4.4 discusses the implementation details. Section 4.5 presents the results of the implementation and shows the performance of the proposed method. Finally, Section 4.6 gives a summary for this chapter.

4.2 Introduction

CBCT are a group of series of DICOM images that present in .dcm format. The CBCT images are complex in nature. Current CBCT devices do not produce calibrated house field unit values (HU). This chapter discusses the methods used to prepare images for further analysis and classification of CBCT images to predict osteoporosis.

4.3 Dataset

Ethical clearance for this study was obtained from Department of Dentomaxillofacial Radiology, Dentistry Faculty, Jordan University Hospital, Amman, Jordan. The research sample will be obtained from patients data consist of CBCT and BMD information that was determined from DEXA. The data will acquire study for women patients with age in the range of 50-85 year old. It is also limited to patient who never took treatments for osteoporosis disease. The patients will be assigned into two

groups; osteoporosis and healthy, using the T-score derives from the DEXA technique that provided by Everest Digital Radiology Center. An example for normal and osteoporotic patient is shown in appendix A, and appendix B.

Everest Digital Radiology Center also provided us with CBCT images of the patients using CS8100 3D carestream health Inc. machine. This system uses rotating anode: 75 kvp and 4 mAs.

4.4 Implementation

Implementation contains 3 phases; image processing, feature extraction, and classification.

4.4.1 Gaussian Filter

The Gaussian function is used to convolve noisy images to get smooth images. Figure 4.1 illustrate the result of applying Gaussian filter to an image of mandible bone as an example.

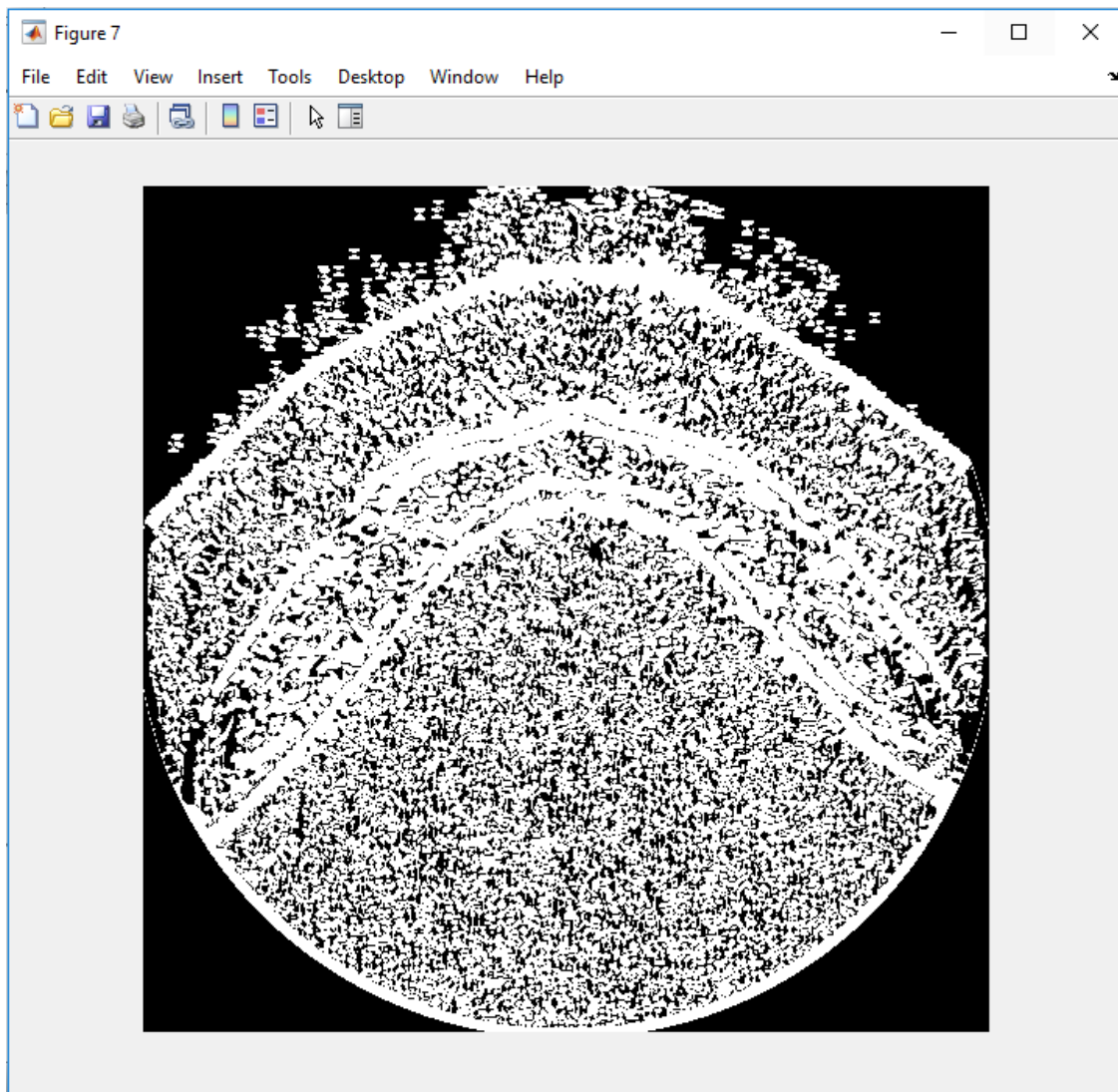


Figure 4.1: The Result of Applying Gaussian Filter.

4.4.2 Binarization

Threshold values are determined by analyzing the histogram of the grayscale image. It is set as a decimal value of 159.

4.4.3 Edge Detection

There is a very large amount of edge detection techniques available. Using Matlab 2018b, several different Edge Detection Methodologies were applied on CBCT image to evaluate the best edge detector, as listed in the following for one image as an example for each edge detection technique.

4.4.3.1 Roberts Edge Detection

Robert edge detection is highly sensitive to noise and it seems not much compatible with CBCT technology which is shown in Figure 4.2.

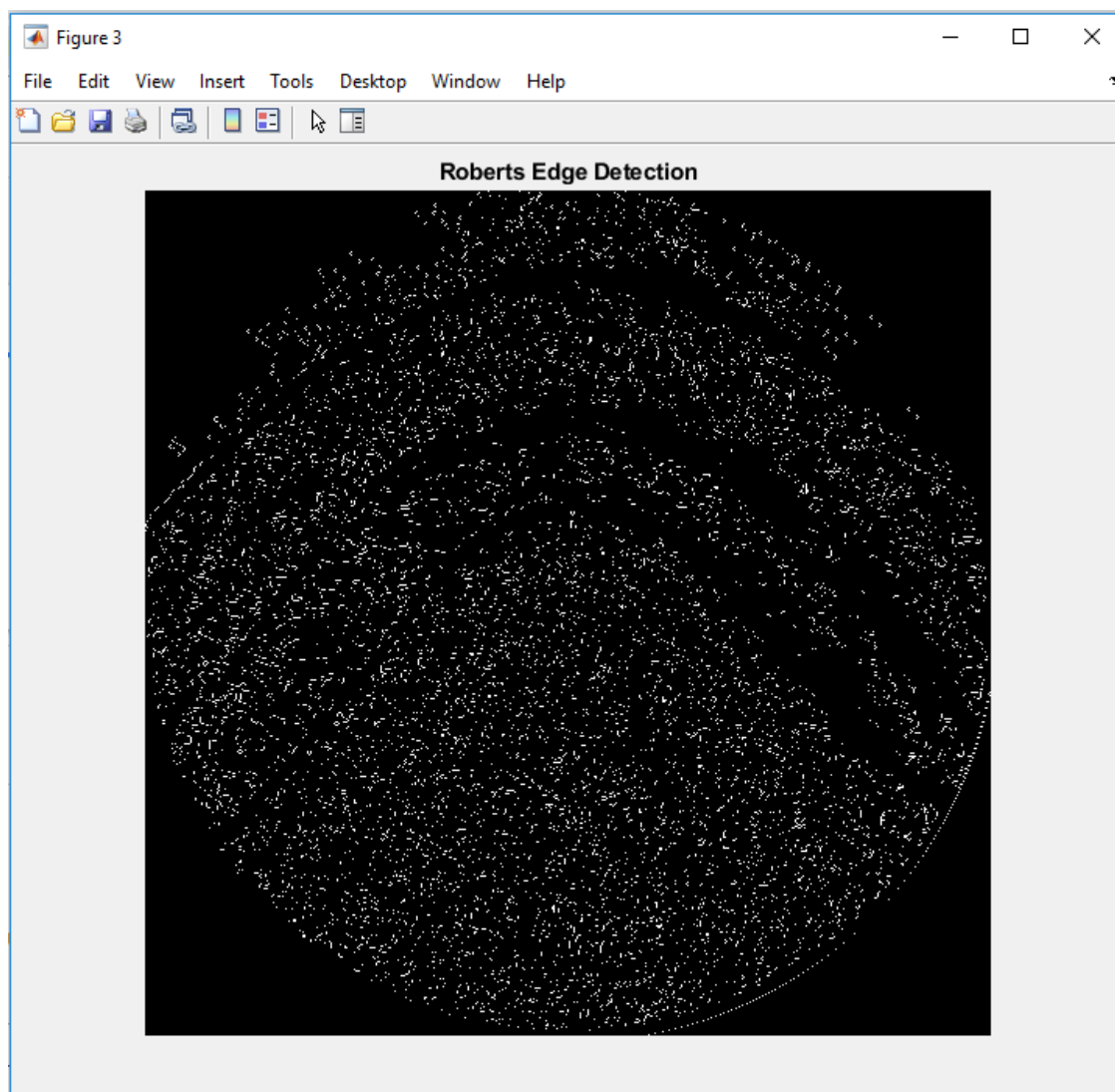


Figure 4.2: Edge Detection Using Matlab2018b Roberts Edge Detection

4.4.3.2 Sobel Edge Detection

The use of Sobel edge detector has shown slow computation ability and less sensitive to noise as compared to Robert operator. Errors due to effects of noise are reduced by local averaging within the neighborhood of the mask the result of applying Sobel edge detection is shown in Figure 4.3.

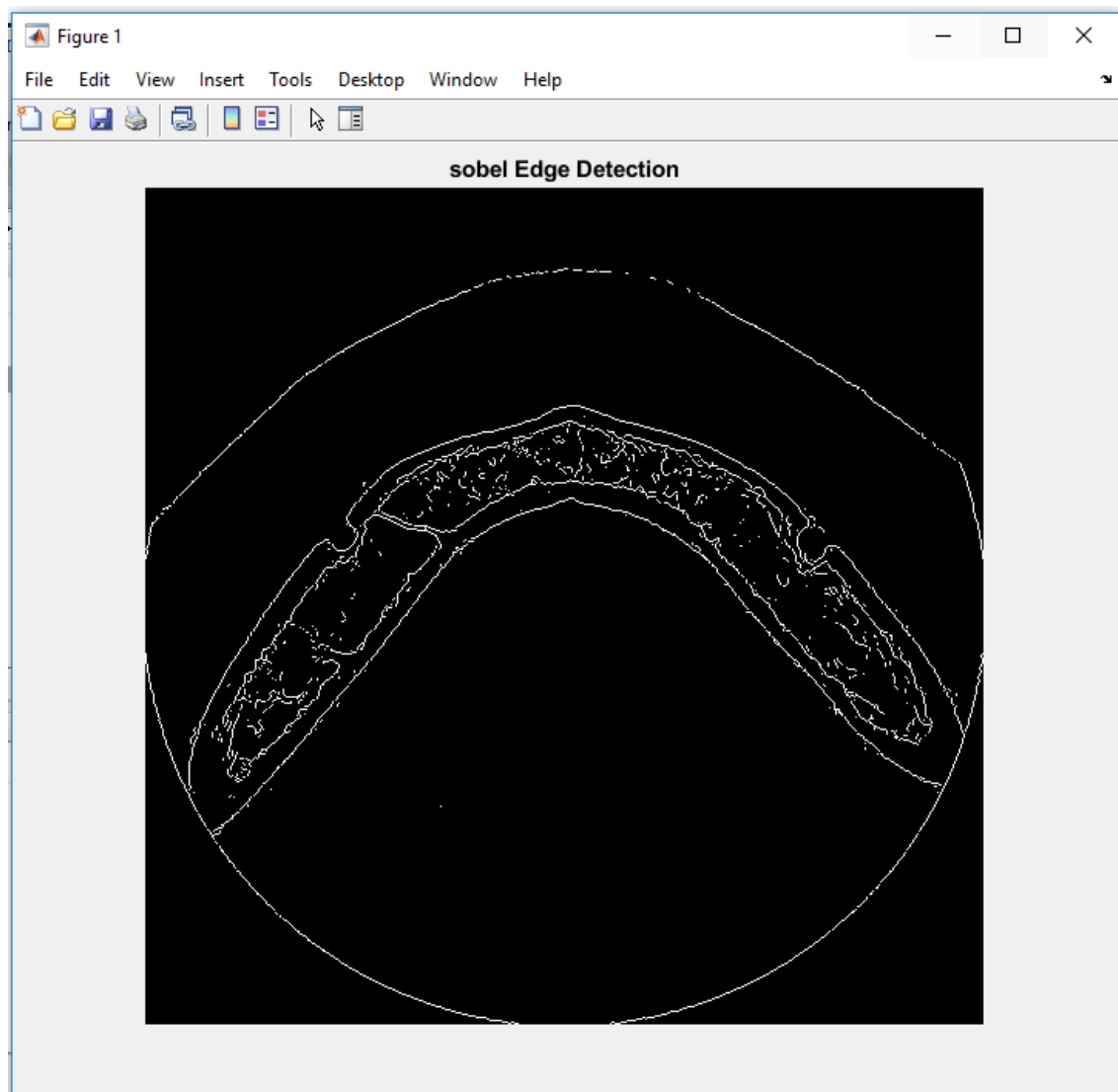


Figure 4.3: Sobel Edge Detection Using Matlab2018b

4.4.3.3 Prewitt Edge Detection

Prewitt edge operator gives better performance on the used images than that of Sobel operator as shown below in Figure 4.4.

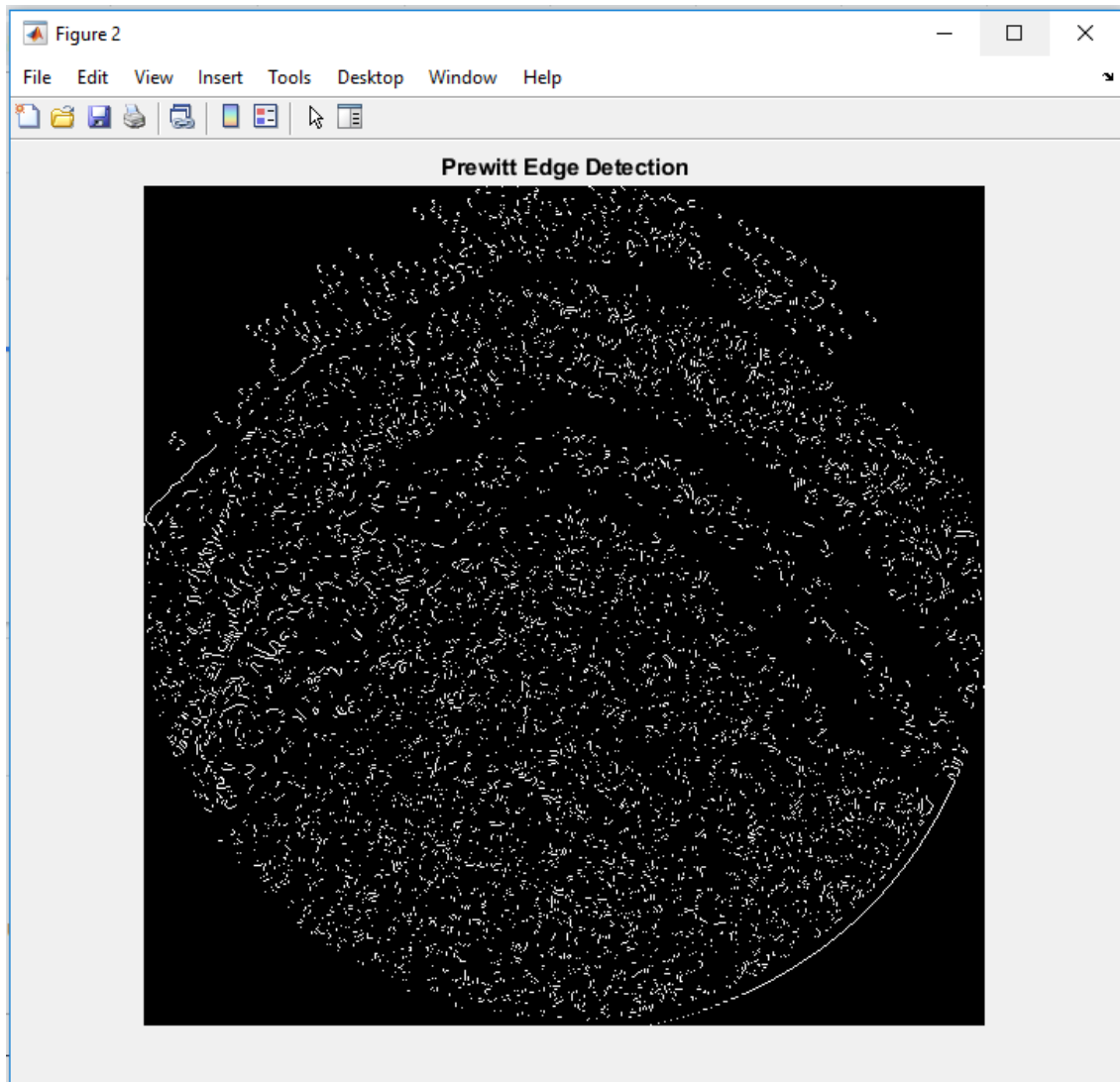


Figure 4.4: Edge Detection Using Matlab2018b Prewitt Edge Detection

4.4.3.4 Canny Edge Detection

Figure 4.5 shows image after applying Matlab2018b canny edge detection.

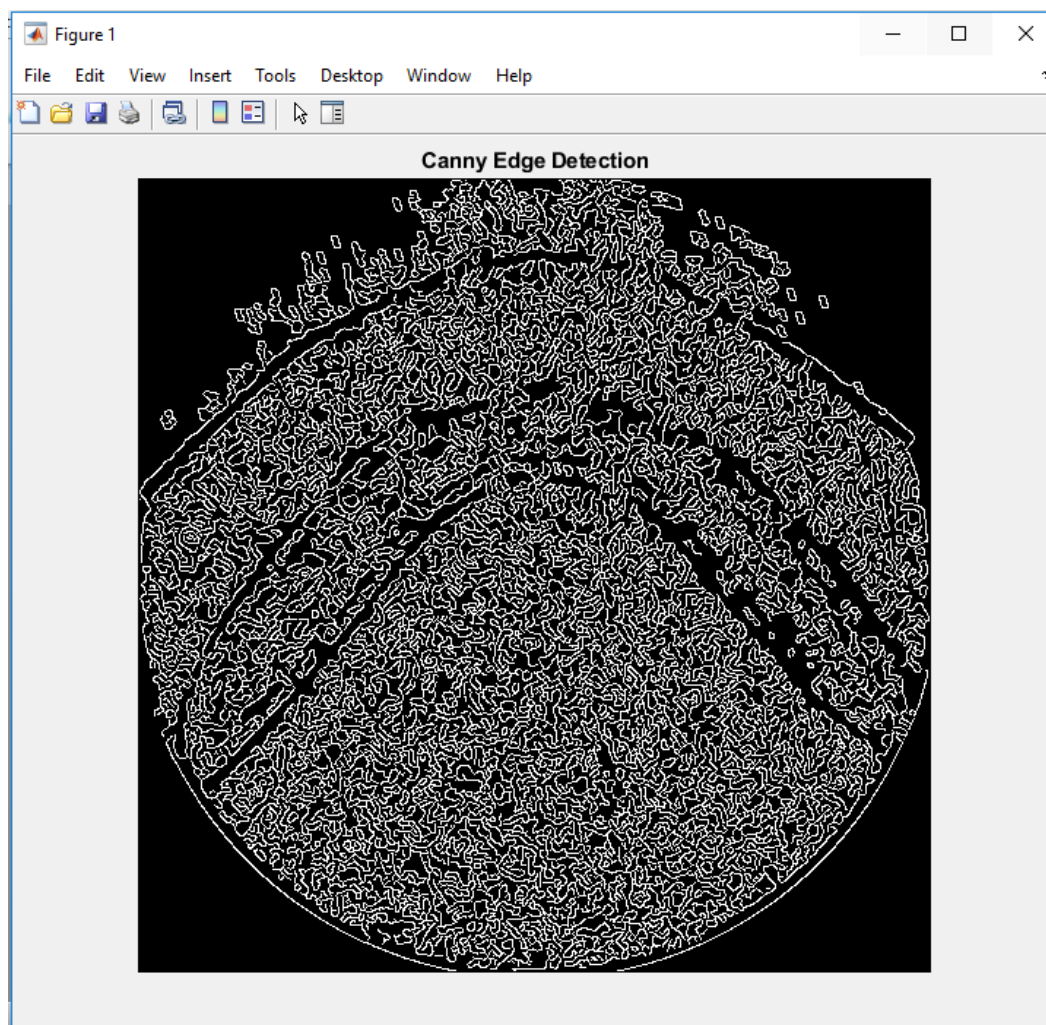


Figure 4.5: Edge Detection Using Canny on Matlab 2018b.

From the figures it is observed that Canny result is best by far to the other results. It is found that Canny's algorithm with threshold that produce the most accurately edge detection from CBCT image, and hence it will be adopted for the rest of the research work.

Figure 4.6 shows edge detection using canny edge with specify threshold.

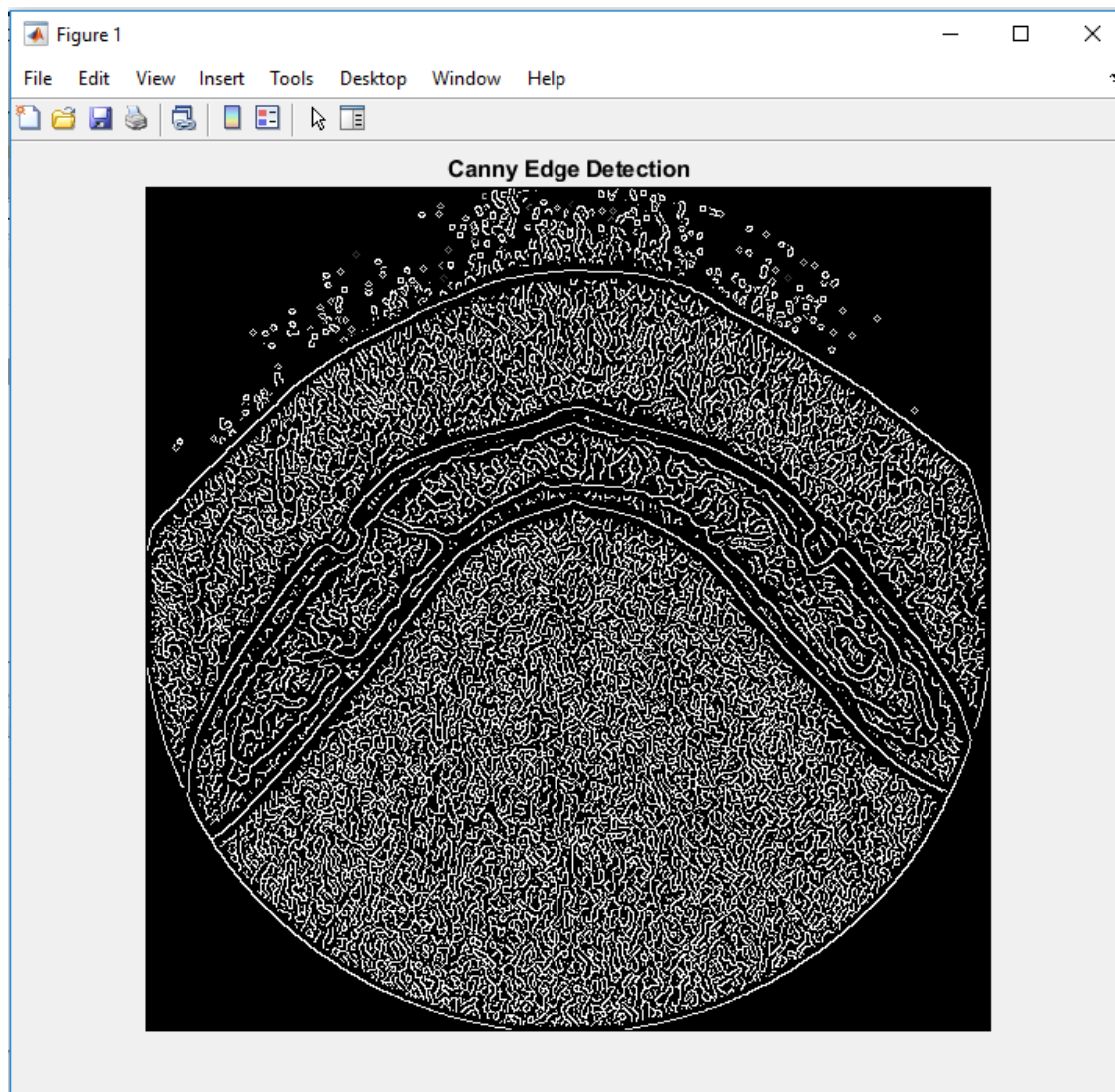


Figure 4.6: Edge Detection Using Canny Edge Detection with Specified Threshold.

It is quite clear that the RoI, or the parts of the image that is of significant for the project is distinguished and isolated from other parts. The investigation will be continued on the relevant part that is confirmed inside the edges while all external parts will be ignored.

4.4.4 Segmentation

After digitally segmenting the image to extract the inner trabecular bone, it will look like the image shown in Figure 4.7, where only the region of interest for the test is left.

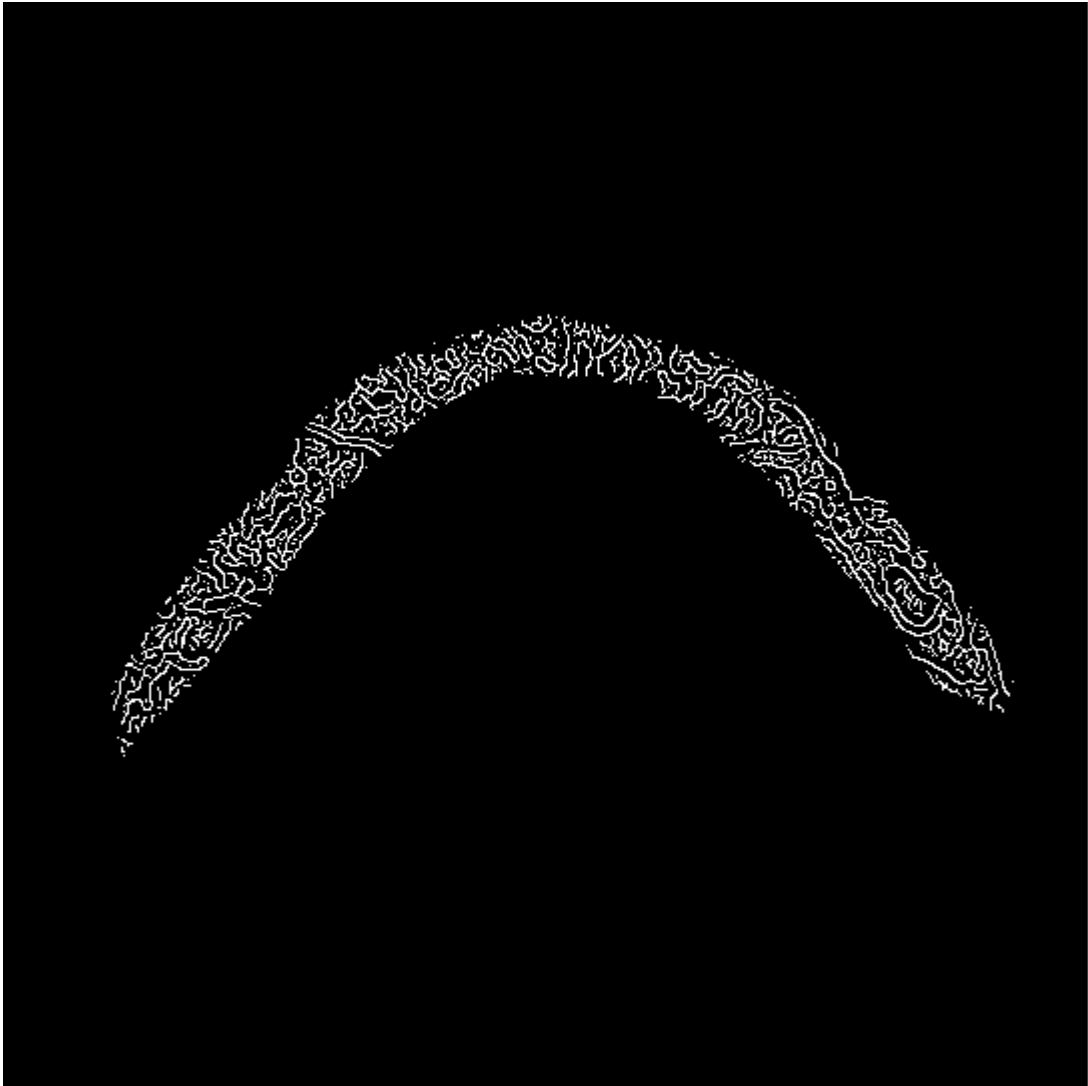


Figure 4.7: Segmented Image.

4.4.5 Filtering Effect and Feature Extraction

Extracting the seven features of interest from the CBCT images (namely; coarseness, contrast, direction, number of non-zero matrix elements, length of edges, number of edges, and the average of one edge length) and applying them directly as input

to the classifier has produces fault results, as normal patients were diagnosed as osteoporotic and vice versa. However, when the same images were processed by some filters and handed over to the modified Tamura texture-based algorithm to extract the required features and finally these features were fed as input to the classifier, the obtained diagnosis results were in complete agreement with the professionally available diagnosis. The image processing filters involved in this process were Gaussian filter, binarization, and canny filter. Table 4.1 depicts few examples for the features obtained directly from the original images without filtering. The feature value shown in red colors are the faulty one, which give faulty diagnoses. On the other side, Table 4.2 lists the feature extracted from the same images of Table 4.1, but the features were extracted after being processed by the filters.

Table 4.1: Feature Extraction from Original Image.

| | Coarseness | Contrast | Directionality | Non- zero pixels | Length of edges | Number of edges | Edge length |
|---------------------|----------------------|---------------------|------------------------|-------------------|------------------|-----------------------|------------------|
| Osteoporotic | 0.000627597693878967 | 0.00906376065147252 | 0.00000000927654494334 | 0.996199542935064 | 1414.22365879219 | 0.0000505044128230704 | 1414.22365879219 |
| | 0.001083020714400040 | 0.01408065934208560 | 0.00000000970035509702 | 0.992247045517875 | 1712.79870183088 | 0.0001311281942008560 | 1712.79870183088 |
| | 0.000706931439028593 | 0.00760021116097634 | 0.00000000937378115578 | 0.995765948138426 | 1157.00220230018 | 0.0000593212169747662 | 1157.00220230018 |
| | 0.000943077870048035 | 0.01098940399882120 | 0.00000000956031731496 | 0.993002523499399 | 1476.16622037092 | 0.0000881571842595347 | 1476.16622037092 |
| Normal | 0.000903198986552948 | 0.01182509539439870 | 0.00000000959067183541 | 0.993730114168070 | 1567.08029197080 | 0.0000935803855511885 | 1567.08029197080 |
| | 0.000529315847968951 | 0.00766271752898813 | 0.00000000896058660535 | 0.996719828073747 | 1322.73484551869 | 0.0000348028851591797 | 1322.73484551869 |
| | 0.000569855142756368 | 0.00753887548409723 | 0.00000000918293770710 | 0.997159750234846 | 1234.88551693651 | 0.0000442062220257501 | 1234.88551693651 |
| | 0.000553811174876549 | 0.00840287023966434 | 0.00000000908919480819 | 0.996450069455163 | 1410.02675641900 | 0.0000398309177541337 | 1410.02675641900 |

Table 4.2: Feature Extraction After Image Pre-Processing.

| | Coarseness | Contrast | Directionality | Non- zero pixels | Length of edges | Number of edges | Edge length |
|---------------------|----------------------|----------------------------|------------------------|--------------------|------------------------|--------------------|------------------|
| Osteoporotic | 0.001949411241947110 | 0.0000089168580239815 0 | 0.00000000950808719039 | 0.9212033270282180 | 733.7945180866920 | 0.0572124478532376 | 2.65867579016918 |
| | 0.003509272159996060 | 0.0000110612296662644 0 | 0.00000000978205793474 | 0.9229455188823140 | 857.4576908119880 | 0.0824842901592337 | 5.07371414681649 |
| | 0.002052553311329180 | 0.0000090139941921873 4 | 0.00000000951191966057 | 0.9237622433919230 | 677.2150233699510 | 0.0751375285120086 | 1.93490006677129 |
| | 0.002748244757632030 | 0.0000100622729231367 0 | 0.00000000967481660104 | 0.9258278145695360 | 1036.807858706440 0 | 0.0801324503311258 | 4.28432999465471 |
| Normal | 0.001479094222485040 | 0.0000079736418102660 5 | 0.00000000923988210915 | 0.9201715596635300 | 593.2417943695260 | 0.0629052099610998 | 1.25421098175375 |
| | 0.001342928573383580 | 0.0000075497265859792 6 | 0.00000000915924645776 | 0.9253455680802100 | 592.9137625211380 | 0.0606264933085120 | 1.14683513060181 |
| | 0.001671776471592850 | 0.0000084991176381344 8 | 0.00000000940671326679 | 0.9222177221665640 | 527.1202132723710 | 0.0617312898343743 | 1.45613318583528 |
| | 0.001601249496223920 | 0.0000082849364666249 2 | 0.00000000934166302073 | 0.9216291268127120 | 750.8100477060900 | 0.0610922554767047 | 1.89598496895477 |

4.4.6 Classification

Classification aims to categorize images into two categories Normal and Osteoporotic.

4.4.6.1 The Proposed Diagnosis Model

A feed-forward back propagation neural network is proposed to diagnose osteoporosis. The neural networks illustration by Matlab 2018b is shown in Figure 4.8.

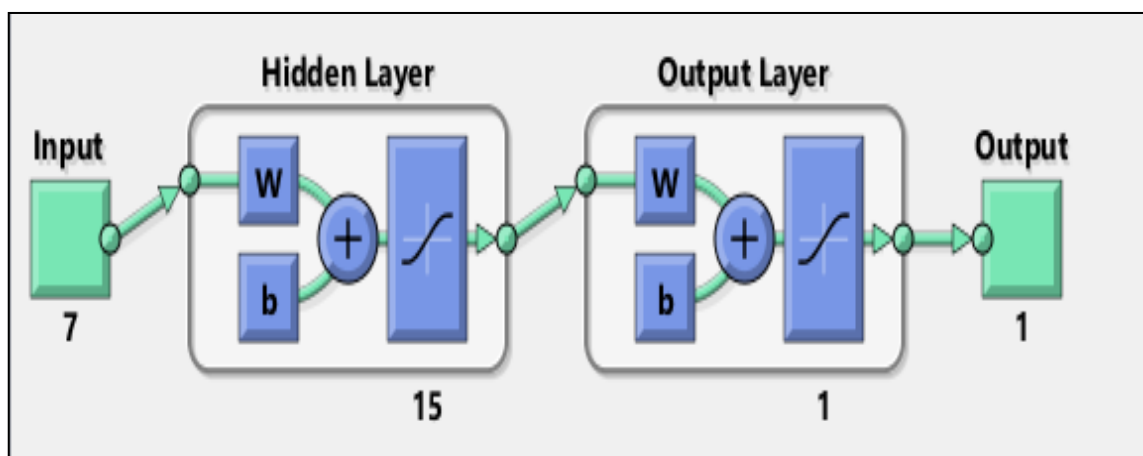


Figure 4.8: Architecture of B-PANN (7:15:1).

4.5 Experimental Results

After implementation we got these results illustrated below:

4.5.1 Data Analysis

Features extracted from mandible CBCT images shown in Table 4.3:

Table 4.3: Definitions of the Used Dataset Variables as Input.

| Input | Parameter |
|-------|------------------------------------|
| P1 | Coarseness |
| P2 | Contrast |
| P3 | Direction |
| P4 | Number of Non-Zero Matrix Elements |
| P5 | Length of Edges |
| P6 | Number of Edges |
| P7 | Average of One Edge Length |

The proposed method has been implemented using Matlab 2018b. Database contains 120 CBCT images, organized in two classes of 60 images: Normal and Osteoporotic, 72 images used for training and 48 images used for testing Figure 4.9 is the confusion matrix for the proposed BP-ANN classifier. Data set is listed in appendix C for normal and osteoporotic. [Note: TN: True Negative, FN: False negative, TP: True positive, and FP: False positive].

| N=48 | Predict: Healthy | Predict: Osteoporotic | Total |
|----------------------|------------------|-----------------------|-------|
| Actual: Healthy | TN=23 | FP=1 | 24 |
| Actual: Osteoporotic | FN=0 | TP=24 | 24 |
| Total no. of images | 23 | 25 | 48 |

Figure 4.9: Confusion Matrix For Classification.

To evaluate the performance of the classifier, basically three metrics can be used, namely; precision, recall and Accuracy. These measures are defined in equations 4.1 to 4.3 (Powers, David &, Ailab, 2011).

$$Accuracy = \frac{\text{Number of Correctly Classified Testing Samples}}{\text{Total Number of Testing Samples}} * 100\% \dots\dots\dots (4.1)$$

$$Precision P = \frac{TP}{Tp+FP} 0 \leq P \leq 1 \dots\dots\dots (4.2)$$

$$Recall(R) = \frac{TP}{TP+FN} 0 \leq R \leq 1 \dots\dots\dots (4.3)$$

Moreover, another metric is also useful for accuracy measurement in binary classification called F1-score (Hand & Christen, 2018) is defined as in equation 4.4

$$F1 = \left(\frac{R^{-1} + P^{-1}}{2} \right)^{-1} = 2 \cdot \frac{P \cdot R}{P + R} 0 \leq F1 \leq 1 \dots\dots\dots (4.4)$$

Evaluating accuracy, precision, recall, and F1-score for the BP-ANN classifier using the above equation resulted in the values summarized in Table 4.4. The classifier converged for 35 epochs.

Table 4.4: The BP-ANN Classifier Performance investigation.

| Testing samples percentage | Accuracy (A) | Precision (P) | Recall (R) | F1-score |
|----------------------------|--------------|---------------|------------|----------|
| 40% from the dataset. | 97.917% | 0.96 | 1 | 0.97959 |

The results of applying the artificial neural networks methodology to distinguish between healthy and Osteoporotic person were very good; the network was able to classify 97.917% of the cases in the testing set. The training state values and best validation and testing performance are shown in Figure 4.10 and Table 4.5. Where the lower values of cross-entropy means better classification while zero means no error.

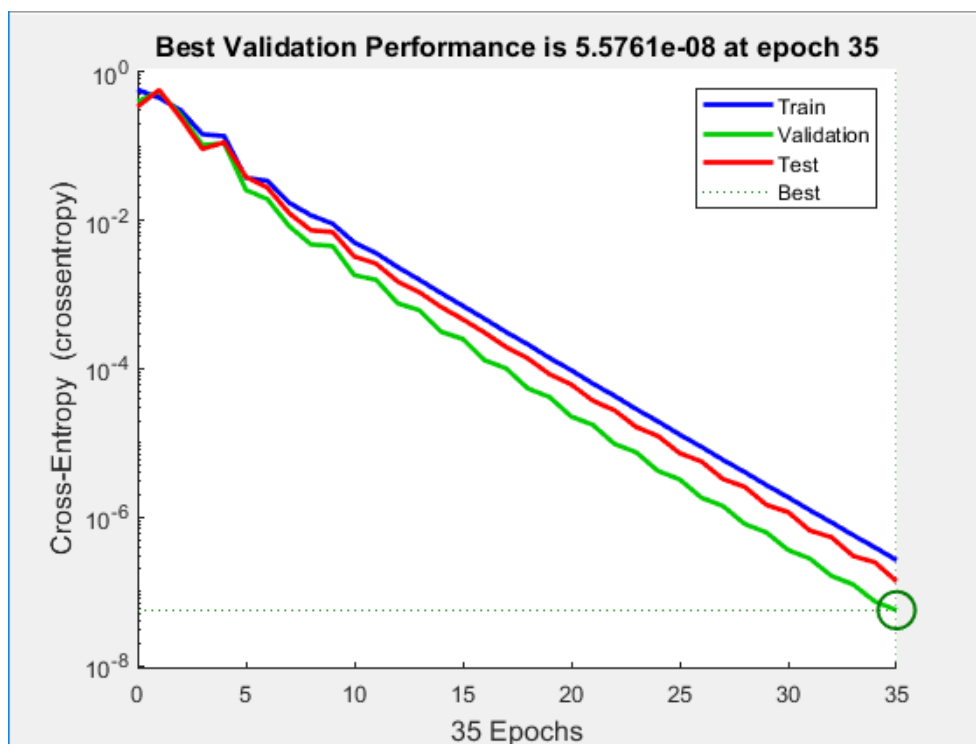


Figure 4.10: Validation Performance.

Table 4.5: Cross-Entropy for the NN as a Function of Number of Epochs.

| Number of epochs | Training | Validation | Testing |
|------------------|-----------|------------|-----------|
| 5 | 0.03862 | 0.02563 | 0.03862 |
| 10 | 0.005012 | 0.001818 | 0.003238 |
| 15 | 0.0007033 | 0.0002521 | 0.0004626 |
| 20 | 9554e-05 | 2.27e-05 | 6.118e-05 |
| 25 | 1.294e-05 | 3.229e-06 | 7.279e-05 |
| 30 | 1.853e-06 | 3.601e-07 | 1.169e-06 |
| 35 | 9e-09 | 5.576e-08 | 9e-09 |

4.6 Summery

The approach based on image processing, feature extraction, and neural network technology, using feed forward neural for classification allowed us to detect osteoporosis from CBCT images.

The performances of the classification algorithm are evaluated using precision, recall, accuracy rate, and F1-score. The results demonstrate the effectiveness of the proposed algorithm.

With the help of the proposed method, dentists will be able to predict osteoporosis accurately and efficiently. This means a great relief on reducing the risk of jaws fracture and dental implant failure.

CHAPTER 5

CONCLUSION AND FUTURE WORK

Chapter Five

Conclusion and Future Work

5.1 Conclusion

This thesis aims at the topic of, using Image Analysis for Mandible Bone Properties on Cone-Beam CT in order to Detect Osteoporosis. It provides a new method to be used for detecting of osteoporosis. CBCT images are mainly used by dentist to evaluate the bone adequacy for dental implants. The mandible trabecular bone has been mainly studied for osteoporosis detection using CBCT images, supplied from a local radiology center.

The proposed scheme represents an approach based on image processing, feature extraction, and artificial neural network technology. Using feed forward B-PANN classifier allows the scheme to detect osteoporosis from CBCT images. The input and target data samples are randomly chosen and automatically divided into 60% as training set, and 40% as validation and test set.

The proposed method was designed, coded, implemented, and tested using Matlab 2018b software tool. The experimental data set consists of a database that contains 120 CBCT image slices, which are organized in two classes of 72 images for training and 48 images for testing. they included both normal and osteoporotic cases.

The performances of the classification algorithm are evaluated using accuracy rate, precision, recall, and F1-score metrics, which resulted into 97.917%, 0.96, 1, and 0.97959, respectively.

The designed classifier converges to the acceptable level and using a best validation performance of 5.5761e-08. This convergence was approached after 35 epochs.

It is worth mentioning that with the help of the proposed scheme, dentists will be able to predict osteoporosis accurately and efficiently. This means a great relief on reducing the risk of jaws fracture and dental implant failure.

Detecting osteoporosis using CBCT images contributions in this thesis can be summarized in the following:

1. Accurate and efficient osteoporosis prediction that assist dentists.
2. Reduces the risk of jaws fracture and dental implant failure.
3. Create an opportunity for early osteoporosis detection, and timely diagnosis, in addition to treatment.
4. Cost reduction in terms of DEXA examination, medicine cost, and patient inconvenient.

5.2 Future Work:

The scheme can be modified or improved by many ways. There improvement may be achieved through various researches and development methods that are summarized in the following.

- 1- To use ANN to choose mandible slice from CBCT image series automatically.
- 2- To use ANN for the segmentation process in order to extract the required relevant features.
- 3- Use the cortical of the mandible in order to extract more features aiming to get more accurate result.
- 4- Look for an algorithm that can be used to unify the efforts for producing homogeneous and matched features when different CBCT source machine of different specification.

5- Look for an algorithm that can be used to estimate the degree of osteoporosis.

REFERENCES

- Ali, M., & Clausi, D. (2002). Using the Canny edge detector for feature extraction and enhancement of remote sensing images. *IEEE*, 00(C), 2298–2300. <https://doi.org/10.1109/igarss.2001.977981>
- Alkhader, M., Aldawodyeh, A., & Abdo, N. (2018). Usefulness of measuring bone density of mandibular condyle in patients at risk of osteoporosis : A cone beam computed tomography study, 363–368. <https://doi.org/10.4103/ejd.ejd>
- Angus, J. E. (1991). Criteria for Choosing the Best Neural Network Part I. *Report No. 91-16, Supported by the Naval Health Research Center under the American Society for Engineering Education Navy Summer Faculty Research Program*, 1–28.
- Badamia, R. H. (2015). Neural Networks in Medical Image Processing. *International Journal of Research in Medical & Applied Sciences*, 1(2), 2454–3667.
- Bagri, N., & Johari, P. (2015). A Comparative Study on Feature Extraction using Texture and Shape for Content Based Image Retrieval. *International Journal of Advanced Science and Technology* (Vol. 80). <https://doi.org/10.14257/ijast.2015.80.04>
- Barnkggei, I., Haffar, I. Al, & Khattab, R. (2014). Osteoporosis prediction from the mandible using cone-beam computed tomography, 263–271.
- Barnkggei, I., Joury, E., & Jawad, A. (2015). An innovative approach in osteoporosis opportunistic screening by the dental practitioner: the use of cervical vertebrae and cone beam computed tomography with its viewer program. *Oral Surgery, Oral Medicine, Oral Pathology and Oral Radiology*, 120(5), 651–659. <https://doi.org/10.1016/j.oooo.2015.08.008>
- Beatriz, M., Cal, C., & Aranha, P. C. (2016). Validation of cone-beam computed tomography as a predictor of osteoporosis using the Klemetti classification, 30(1), 1–8. <https://doi.org/10.1590/1807-3107BOR-2016.vol30.0073>
- Buscema, Massimo. (1998). Back Propagation Neural Networks. *Substance use & misuse*. 33. 233-70. [10.3109/10826089809115863](https://doi.org/10.3109/10826089809115863).
- Camargo, A. J., Rodriguez, A., Côrtes, G., Aoki, E. M., Baladi, M. G., Arita, E. S., ... Watanabe, A. (2016). Analysis of Bone Quality on Panoramic Radiograph in Osteoporosis Research by Fractal Dimension, (March), 375–386.
- Esmaeli, F., Payahoo, S., Mobasser, M., Johari, M., & Yazdani, J. (2017). Efficacy of radiographic density values of the first and second cervical vertebrae recorded by CBCT technique to identify patients with osteoporosis and osteopenia. *Tabriz University of Medical Sciences*, 11(3), 189–194. <https://doi.org/10.15171/joddd.2017.034>

- Fontaine, E., & Lee, H. S. (2002). Optimizing Katsevich Image Reconstruction Algorithm on Multicore Processors.
- Gedraite, E. S., & Hadad, M. (2011). *Investigation on the Effect of a Gaussian Blur in Image Filtering and Segmentation. Proceedings ELMAR-2011.*
- Gijsbert, B., & van der, V. (2011). Bone Mineral Content. *Side Effects of Drugs Annual.*
- Gonzalez, R. C., & Woods, R. E. (2018). *Digital image processing.* New York, NY: Pearson.
- Gueld, M. O., Keyzers, D., Deselaers, T., Leisten, M., Schubert, H., Ney, H., & Lehmann, T. M. (2004). Comparison of global features for categorization of medical images. *Medical Imaging*, 5371(i), 211–222. <https://doi.org/10.1117/12.535914>
- Güngör, E., Yildirim, D., & Çevik, R. (2016). *Evaluation of osteoporosis in jaw bones using cone beam CT and dual-energy X-ray absorptiometry. Journal of Oral Science* (Vol. 58). <https://doi.org/10.2334/josnugd.15-0609>
- Hand, D., & Christen, P. (2018). A note on using the F-measure for evaluating record linkage algorithms. *Statistics and Computing*, 28(3), 539–547. <https://doi.org/10.1007/s11222-017-9746-6>
- HECHT-NIELSEN, R., 1987, Kolmogorov's mapping neural network existence theorem. *IEEE First Annual International Conference on Neural Networks*, 3, pp. 11–13.
- Held, D. (2017). Analysis of 3D Cone-Beam CT Image Reconstruction Performance on a FPGA. In *Proceedings of the 2017 International Conference on Biomedical Engineering and Science* (pp. 3–9). <https://doi.org/10.1080/2201473X.2014.1001307>
- Home. (n.d.). Retrieved December 13, 2018, <<glossary>> . (Online), available: <https://americanbonehealth.org/glossary/>
- Hwang, J. J., Lee, J. H., Han, S. S., Kim, Y. H., Jeong, H. G., Choi, Y. J., & Park, W. (2017). Strut analysis for osteoporosis detection model using dental panoramic radiography. *Dentomaxillofacial Radiology*. <https://doi.org/10.1259/dmfr.20170006>
- Inglot, J., & Technology, I. (2012). *Advanced Image Processing with Matlab*, (May 2012).
- Journal, I., & Sciences, A. M. (n.d.). BLOCK PROCESSING AND EDGE DETECTION. *International Journal of Pure and Applied Mathematical Sciences (IJPAMS) [SCOPUS]*, 9(1), 9–16.
- Kannan, Kumar, P. S. (2015). Cone Beam Computed Tomography Evaluation of Postmenopausal Alveolar Bone Changes in Osteoporotic Women. *International Journal of Oral Implantology and Clinical Research*, 6(3), 65–68.

- Klintström, E. (2017). *Image Analysis for Trabecular Bone Properties on Cone-Beam CT Data*.
- Koh, K., & Kim, K. (2011). Utility of the computed tomography indices on cone beam computed tomography images in the diagnosis of osteoporosis in women, 101–106.
- Krig, S. (1993). Image pre-processing. *Computer Vision Metrics*, 56–111. https://doi.org/10.1007/978-3-319-50490-2_3
- Kulkarni, R., & Bhavani k. (2018). A Survey on Noise Reduction and Segmentation Techniques in CT DICOM Images. *International Research Journal of Engineering and Technology (IRJET)*, 05(05), 424–427.
- Majtner, T., & Svoboda, D. (2009). Extension of Tamura Texture Features for 3D Fluorescence Microscopy a s.
- Mandible Anatomy, Definition & Function | Body Maps. (n.d.).(Online). Retrieved from <https://www.healthline.com/human-body-maps/mandible#1>
- Mayil, M., Keser, G., & Pekiner, F. N. (2014). CBCT Images of Anatomic Landmarks in Maxillofacial Region, 4(4), 232–240. <https://doi.org/10.5455/musbed.20140814010458>
- McDonnell, P., McHugh, P. E., & O'Mahoney, D. (2007). Vertebral osteoporosis and trabecular bone quality. *Annals of Biomedical Engineering*, 35(2), 170–189. <https://doi.org/10.1007/s10439-006-9239-9>
- Mustra, M., Delac, K., & Grgic, M. (2008). Overview of the DICOM Standard. *ELMAR, 2008. 50th International Symposium*, 1(September), 39–44. <https://doi.org/10.4324/9780203860366>
- Muthukrishnan, & Radha. (2011). EDGE DETECTION TECHNIQUES FOR IMAGE SEGMENTATION. *International Journal of Computer Science & Information Technology (IJCSIT)*, 3(6), 259–267.
- Panchal, F. S., & Panchal, M. (2014). Review on Methods of Selecting Number of Hidden Nodes in Artificial Neural Network. *International Journal of Computer Science and Mobile Computing*, 3(11), 455–464.
- Petersen, Ridder, Handels. (2002). Image processing with neural networks—a review. *Pattern Recognition*, 35(10), 2279–2301. [https://doi.org/10.1016/S0031-3203\(01\)00178-9](https://doi.org/10.1016/S0031-3203(01)00178-9)
- Powers, David & , Ailab. (2011). Evaluation: From precision, recall and F-measure to ROC, informedness, markedness & correlation. *J. Mach. Learn. Technol.* 2. 2229–3981. 10.9735/2229-3981.
- Rashmi, Kumar, M., & Saxena, R. (2013). a Lgorithm a Nd T Echnique on V Arious E Dge D Etection : a S Urvey. *An International Journal (SIPIJ)*, 4(3), 65–75.

- Rice, S.R., Price, G., Morley, S., & Beale, T. (2015). Dental Implant Planning using Cone Beam CT imaging : a pictorial guide ., 1–32.
- Roy, S. (2013). A New Efficient Binarization Method for MRI of Brain Image. *Signal & Image Processing: An International Journal*, 3(6), 35–51. <https://doi.org/10.5121/sipij.2012.3604>
- Shah, S., Haque, S. M. A., Islam, R., Ali, A., & Shabbir, M. (2010). Automatic Recognition of Handwritten Bangla Courtesy Amount on Bank Checks, 10(12), 154–163.
- Shameena, N., & Jabbar, R. (2014). Techniques on Cardiac Medical Images. *International Journal of Engineering Research & Technology (IJERT)*, 3(4), 336–341.
- Shi, J., Lee, S., Pan, H. C., Mohammad, A., Lin, A., Guo, W., ... Kwak, J. H. (2017). Association of Condylar Bone Quality with TMJ Osteoarthritis. *Journal of Dental Research*, 96(8), 888–894. <https://doi.org/10.1177/0022034517707515>
- Suprijanto, Azhari, Juliastuti, E., Septyvergy, A., & Setyagar, N. P. P. (2016). Dental panoramic image analysis for enhancement biomarker of mandibular condyle for osteoporosis early detection Dental panoramic image analysis for enhancement biomarker of mandibular condyle for osteoporosis early detection. In *Journal of Physics: Conference Series 694 (2016) 012066*. <https://doi.org/10.1088/1742-6596/694/1/012066>
- Tinoco, H. A., & Gomez, J. P. (2017). Bone mineral density. *Current Trends in Biomedical Engineering & Biosciences*, 82(1), 62–66. <https://doi.org/10.2319/031811-192.1>
- Tiwari, H. (2017). A review paper on medical image processing. *International Journal of Research - GRANTHAALAYAH*, 5, 21–29.
- Yuvaraju, M., & Haripriya, R. (2018). Calculation of bone Disease using Image Processing. *International Journal of Scientific Research in Computer Science, Engineering and Information Technology*, 4(5), 81–87.

APPENDIX A

DEXA SCAN EXAMPLE FOR NORMAL PATIENT

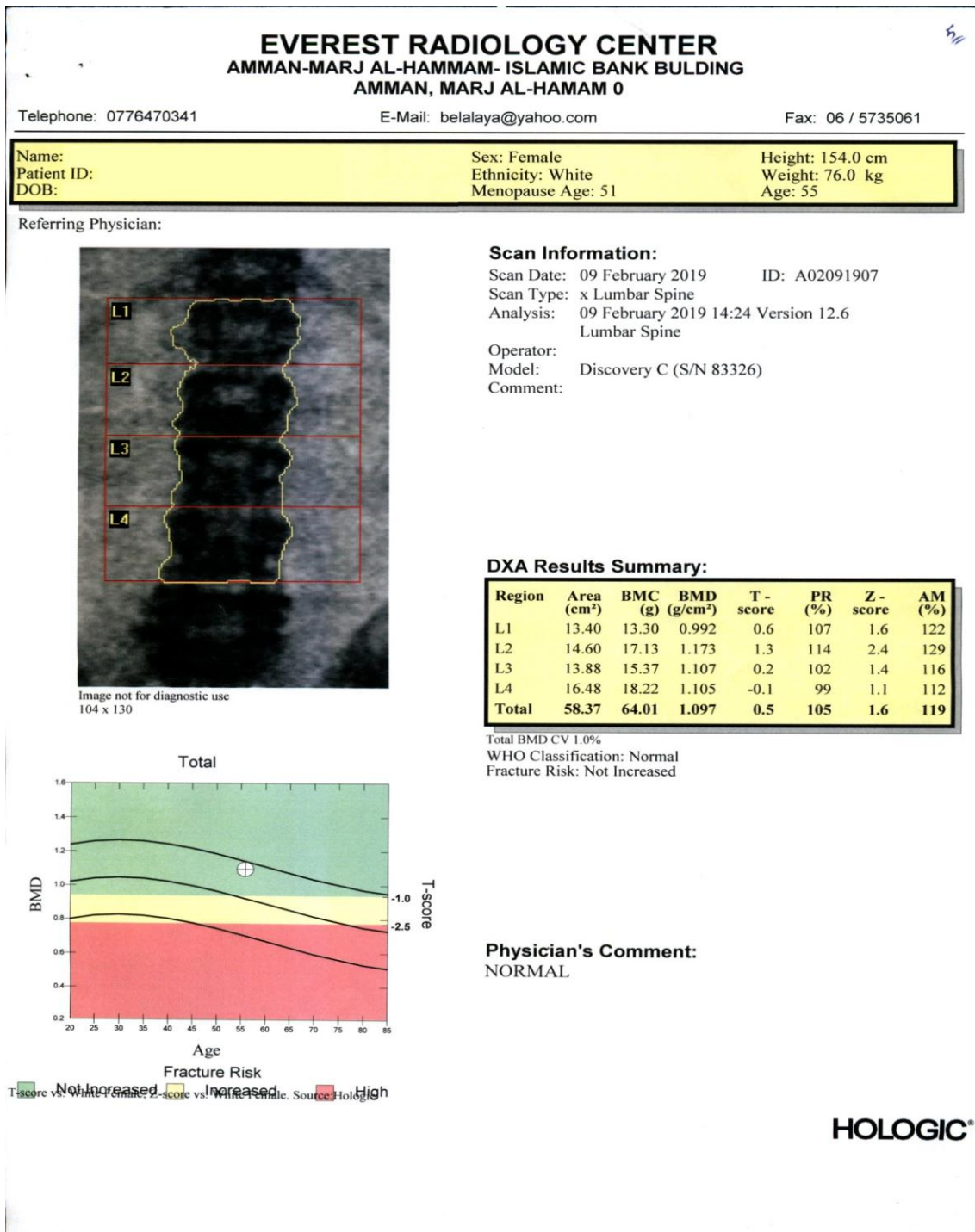


Figure A-1: DEXA Scan For Normal Patient x (page 1).

EVEREST RADIOLOGY CENTER
AMMAN-MARJ AL-HAMMAM- ISLAMIC BANK BULDING
AMMAN, MARJ AL-HAMAM 0

Telephone: 0776470341

E-Mail: belalaya@yahoo.com

Fax: 06 / 5735061

| | | |
|-------------|-------------------|------------------|
| Name: | Sex: Female | Height: 154.0 cm |
| Patient ID: | Ethnicity: White | Weight: 76.0 kg |
| DOB: | Menopause Age: 51 | Age: 55 |

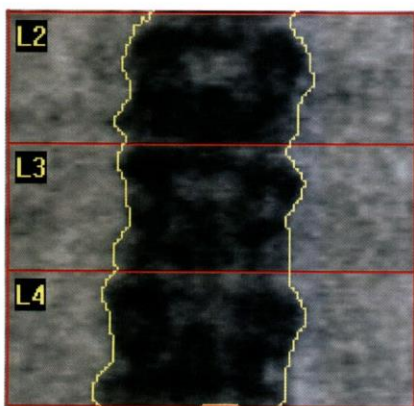


Image not for diagnostic use
104 x 130

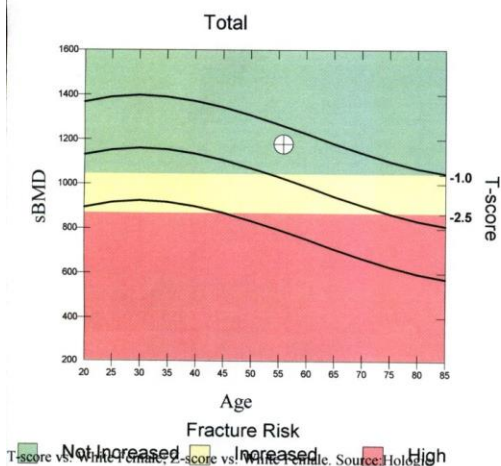
Scan Information:

Scan Date: 09 February 2019 ID: A02091907
 Scan Type: x Lumbar Spine
 Analysis: 09 February 2019 14:24 Version 12.6
 Lumbar Spine
 Operator:
 Model: Discovery C (S/N 83326)
 Comment:

DXA Results Summary:

| Region | sBMD (mg/cm ³) | T - score | PR (%) | Z - score | AM (%) |
|--------|----------------------------|-----------|--------|-----------|--------|
| Total | 1213 | 0.4 | 105 | 1.6 | 118 |

Total BMD CV 1.0%
 WHO Classification: Normal
 Fracture Risk: Not Increased



Physician's Comment:
 NORMAL

HOLOGIC®

Figure A-2: DEXA Scan for Normal Patient x (page 2).

EVEREST RADIOLOGY CENTER
AMMAN-MARJ AL-HAMMAM- ISLAMIC BANK BUILDING
AMMAN, MARJ AL-HAMAM 0

Telephone: 0776470341

E-Mail: belalaya@yahoo.com

Fax: 06 / 5735061

| | | |
|-------------|-------------------|------------------|
| Name: | Sex: Female | Height: 154.0 cm |
| Patient ID: | Ethnicity: White | Weight: 76.0 kg |
| DOB: | Menopause Age: 51 | Age: 55 |

Referring Physician:

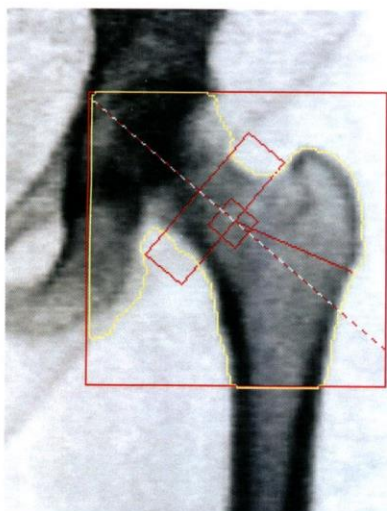


Image not for diagnostic use
 92 x 90
 NECK: -49 x 15

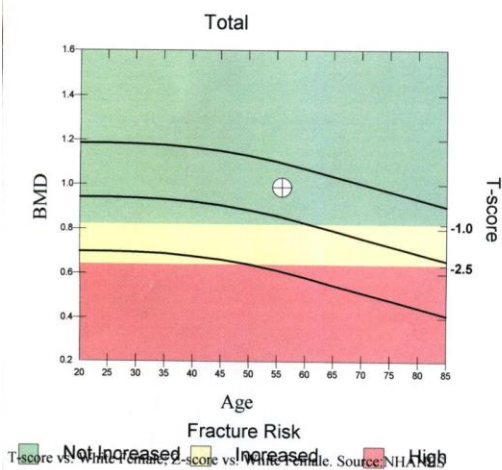
Scan Information:

Scan Date: 09 February 2019 ID: A02091908
 Scan Type: x Left Hip
 Analysis: 09 February 2019 14:23 Version 12.6
 Left Hip
 Operator:
 Model: Discovery C (S/N 83326)
 Comment:

DXA Results Summary:

| Region | Area (cm ²) | BMC (g) | BMD (g/cm ²) | T - score | PR (%) | Z - score | AM (%) |
|--------------|-------------------------|--------------|--------------------------|------------|------------|------------|------------|
| Neck | 4.82 | 4.67 | 0.969 | 1.1 | 114 | 2.2 | 133 |
| Total | 30.08 | 29.70 | 0.987 | 0.4 | 105 | 1.1 | 116 |

Total BMD CV 1.0%
 WHO Classification: Normal
 Fracture Risk: Not Increased



Physician's Comment:

NORMAL

HOLOGIC®

Figure A-3: DEXA Scan for Normal Patient x (page 3).

APPENDIX B

DEXA SCAN EXAMPLE FOR OSTEOPOROTIC PATIENT

EVEREST RADIOLOGY CENTER
AMMAN-MARJ AL-HAMMAM- ISLAMIC BANK BUILDING
AMMAN, MARJ AL-HAMAM 0

Telephone: 0776470341 E-Mail: belalaya@yahoo.com Fax: 06 / 5735061

| | | |
|-------------|-------------------|------------------|
| Name: | Sex: Female | Height: 160.0 cm |
| Patient ID: | Ethnicity: White | Weight: 63.0 kg |
| DOB: | Menopause Age: 50 | Age: 52 |

Referring Physician:

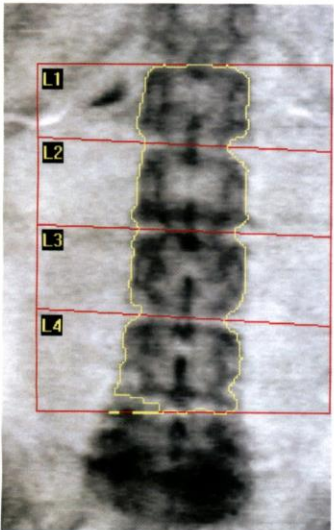


Image not for diagnostic use
113 x 133

Scan Information:

Scan Date: 16 February 2019 ID: A02161907
 Scan Type: x Lumbar Spine
 Analysis: 16 February 2019 13:26 Version 12.6
 Lumbar Spine

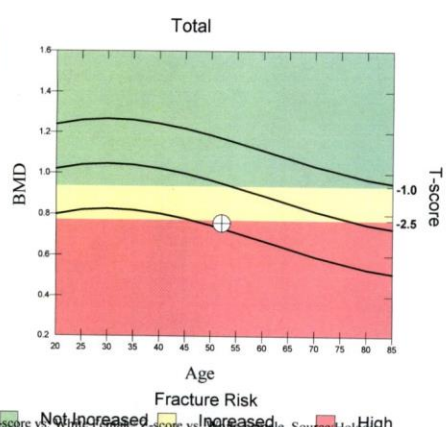
Operator:
 Model: Discovery C (S/N 83326)
 Comment:

DXA Results Summary:

| Region | Area (cm ²) | BMC (g) | BMD (g/cm ²) | T - score | PR (%) | Z - score | AM (%) |
|--------------|-------------------------|--------------|--------------------------|-------------|-----------|-------------|-----------|
| L1 | 11.87 | 7.62 | 0.642 | -2.6 | 69 | -1.8 | 76 |
| L2 | 12.98 | 10.55 | 0.813 | -2.0 | 79 | -1.1 | 87 |
| L3 | 13.67 | 11.06 | 0.809 | -2.5 | 75 | -1.6 | 82 |
| L4 | 14.92 | 11.24 | 0.754 | -3.3 | 68 | -2.4 | 74 |
| Total | 53.44 | 40.48 | 0.757 | -2.6 | 72 | -1.8 | 80 |

Total BMD CV 1.0%
 WHO Classification: Osteoporosis
 Fracture Risk: High

Physician's Comment:
 LOWER LIMIT OF OSTEOPOROSIS



T-score vs. White Female, Z-score vs. White Female. Source: Hologic

HOLOGIC®

Figure B-1 : DEXA Scan for Osteoporotic Patient y, (page 1).

EVEREST RADIOLOGY CENTER
AMMAN-MARJ AL-HAMMAM- ISLAMIC BANK BULDING
AMMAN, MARJ AL-HAMAM 0

Telephone: 0776470341

E-Mail: belalaya@yahoo.com

Fax: 06 / 5735061

| | | |
|-------------|-------------------|------------------|
| Name: | Sex: Female | Height: 160.0 cm |
| Patient ID: | Ethnicity: White | Weight: 63.0 kg |
| DOB: | Menopause Age: 50 | Age: 52 |

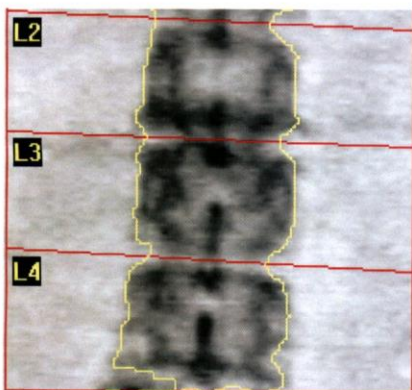


Image not for diagnostic use
113 x 133

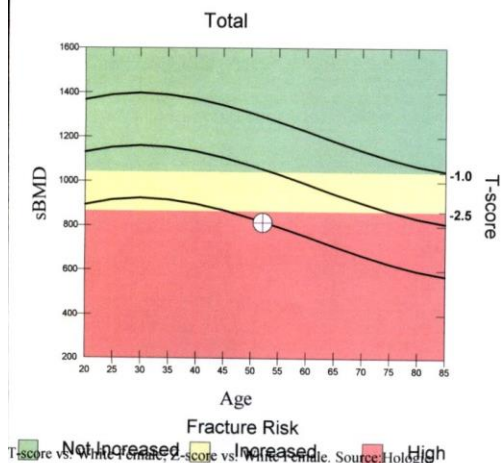
Scan Information:

Scan Date: 16 February 2019 ID: A02161907
 Scan Type: x Lumbar Spine
 Analysis: 16 February 2019 13:26 Version 12.6
 Lumbar Spine
 Operator:
 Model: Discovery C (S/N 83326)
 Comment:

DXA Results Summary:

| Region | sBMD (mg/cm ³) | T-score | PR (%) | Z-score | AM (%) |
|--------|----------------------------|---------|--------|---------|--------|
| Total | 850 | -2.6 | 73 | -1.7 | 81 |

Total BMD CV 1.0%
 WHO Classification: Osteoporosis
 Fracture Risk: High



Physician's Comment:

LOWER LIMIT OF OSTEOPOROSIS

HOLOGIC®

Appendix B-2 : DEXA Scan for Osteoporotic Patient y, (page 2).

EVEREST RADIOLOGY CENTER
AMMAN-MARJ AL-HAMMAM- ISLAMIC BANK BULDING
AMMAN, MARJ AL-HAMAM 0

Telephone: 0776470341

E-Mail: belalaya@yahoo.com

Fax: 06 / 5735061

| | | |
|-------------|-------------------|------------------|
| Name: | Sex: Female | Height: 160.0 cm |
| Patient ID: | Ethnicity: White | Weight: 63.0 kg |
| DOB: | Menopause Age: 50 | Age: 52 |

Referring Physician:

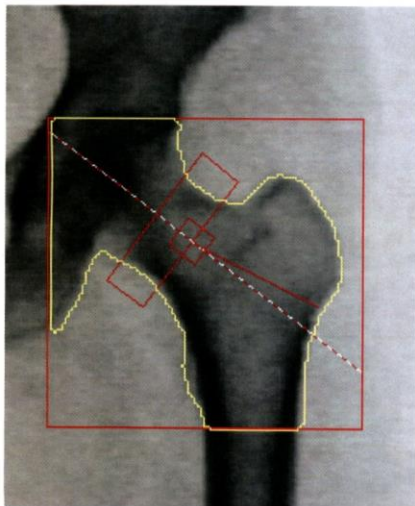


Image not for diagnostic use
 97 x 95
 NECK: -49 x 15

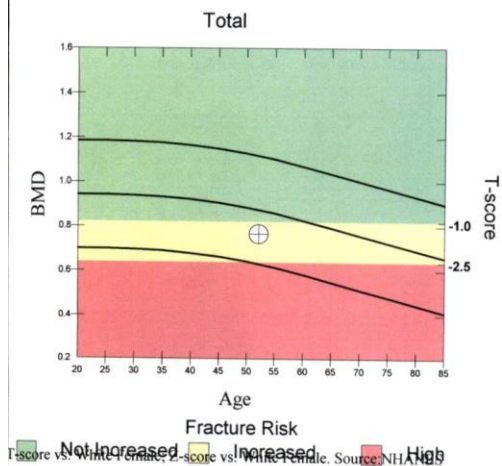
Scan Information:

Scan Date: 16 February 2019 ID: A02161908
 Scan Type: x Left Hip
 Analysis: 16 February 2019 13:25 Version 12.6
 Left Hip
 Operator:
 Model: Discovery C (S/N 83326)
 Comment:

DXA Results Summary:

| Region | Area (cm ²) | BMC (g) | BMD (g/cm ²) | T - score | PR (%) | Z - score | AM (%) |
|--------------|-------------------------|--------------|--------------------------|-------------|-----------|-------------|-----------|
| Neck | 4.65 | 3.35 | 0.721 | -1.2 | 85 | -0.3 | 96 |
| Total | 34.21 | 26.23 | 0.767 | -1.4 | 81 | -0.9 | 88 |

Total BMD CV 1.0%
 WHO Classification: Osteopenia
 Fracture Risk: Increased



Physician's Comment:

LOWER LIMIT OF OSTEOPENIA

HOLOGIC®

Figure B-3 : DEXA Scan for Osteoporotic Patient y, (page 3).

APPENDIX C

IMAGES FEATURES DATA SET

Table C-1: Images Features Data Set for Normal patient

| COARSNESS | contrast | Fdirection | edgePixels | lengthOfEdges | NUMBER OF EDGES | EDGE LENGTH |
|------------------|-----------------|-------------------|-------------------|----------------------|------------------------|--------------------|
| 0.001342929 | 7.55E-06 | 9.16E-09 | 0.92534557 | 592.9137625 | 0.060626493 | 1.146835131 |
| 0.001358632 | 7.60E-06 | 9.18E-09 | 0.92486734 | 571.8853042 | 0.061263869 | 1.125758473 |
| 0.00136112 | 7.59E-06 | 9.18E-09 | 0.9245555 | 569.1238506 | 0.063070639 | 1.08404543 |
| 0.0013734 | 7.63E-06 | 9.19E-09 | 0.92579139 | 576.530425 | 0.06312769 | 1.11514589 |
| 0.001671776 | 8.50E-06 | 9.41E-09 | 0.92221772 | 527.1202133 | 0.06173129 | 1.456133186 |
| 0.001706261 | 8.52E-06 | 9.41E-09 | 0.92241416 | 525.6915347 | 0.063757377 | 1.420787932 |
| 0.001686952 | 8.52E-06 | 9.40E-09 | 0.9233536 | 543.3017887 | 0.067483086 | 1.37893855 |
| 0.001683597 | 8.49E-06 | 9.40E-09 | 0.9212657 | 555.8999185 | 0.062052405 | 1.523013475 |
| 0.001690461 | 8.49E-06 | 9.41E-09 | 0.92058623 | 563.5679152 | 0.058963872 | 1.628809004 |
| 0.001601249 | 8.28E-06 | 9.34E-09 | 0.92162913 | 750.8100477 | 0.061092255 | 1.895984969 |
| 0.00164118 | 8.35E-06 | 9.36E-09 | 0.92325968 | 732.7377972 | 0.064623426 | 1.795925974 |
| 0.0016361 | 8.37E-06 | 9.37E-09 | 0.92127647 | 760.8823261 | 0.061933201 | 1.97631773 |
| 0.001627802 | 8.34E-06 | 9.35E-09 | 0.92288857 | 766.4836914 | 0.06998282 | 1.730211493 |
| 0.001631237 | 8.34E-06 | 9.35E-09 | 0.9232409 | 764.8731309 | 0.062844173 | 1.921791786 |
| 0.001479094 | 7.97E-06 | 9.24E-09 | 0.92017156 | 593.2417944 | 0.06290521 | 1.254210982 |
| 0.001479094 | 7.97E-06 | 9.24E-09 | 0.92017156 | 593.2417944 | 0.06290521 | 1.254210982 |
| 0.001491042 | 7.97E-06 | 9.24E-09 | 0.91958141 | 550.4972363 | 0.062092641 | 1.176276146 |
| 0.001511426 | 8.01E-06 | 9.26E-09 | 0.91870126 | 522.078284 | 0.061029274 | 1.162757871 |
| 0.001501536 | 7.98E-06 | 9.24E-09 | 0.92195235 | 537.9557659 | 0.062730505 | 1.139736792 |
| 0.001452295 | 7.92E-06 | 9.22E-09 | 0.92218354 | 540.6516092 | 0.060572034 | 1.145448325 |

| | | | | | | |
|-------------|----------|----------|------------|-------------|-------------|-------------|
| 0.001500324 | 7.97E-06 | 9.24E-09 | 0.92275855 | 540.0195068 | 0.059520095 | 1.192096042 |
| 0.001462417 | 7.90E-06 | 9.21E-09 | 0.92175551 | 519.1153378 | 0.060539298 | 1.095180038 |
| 0.001425849 | 7.84E-06 | 9.18E-09 | 0.92237936 | 537.1159051 | 0.064033559 | 1.034905405 |
| 0.001451679 | 7.85E-06 | 9.19E-09 | 0.92292904 | 511.7325589 | 0.061520334 | 1.031718869 |
| 0.00141463 | 7.80E-06 | 9.16E-09 | 0.9226406 | 522.9027014 | 0.060704803 | 1.039567995 |
| 0.001425865 | 7.82E-06 | 9.18E-09 | 0.92090578 | 509.5934163 | 0.057679595 | 1.086553126 |
| 0.001373346 | 7.75E-06 | 9.15E-09 | 0.92064103 | 541.5867713 | 0.060847305 | 1.053670761 |
| 0.001369442 | 7.72E-06 | 9.14E-09 | 0.92164613 | 550.5195241 | 0.059056033 | 1.083699851 |
| 0.001390533 | 7.78E-06 | 9.15E-09 | 0.92307692 | 536.6995906 | 0.063021316 | 1.018405295 |
| 0.00139473 | 7.67E-06 | 9.21E-09 | 0.92623961 | 582.0717211 | 0.061391605 | 1.183072604 |
| 0.00135579 | 7.64E-06 | 9.20E-09 | 0.92591173 | 575.8609241 | 0.061073383 | 1.156347237 |
| 0.00140608 | 7.75E-06 | 9.24E-09 | 0.92643193 | 561.8379318 | 0.058153497 | 1.254102526 |
| 0.001329431 | 7.54E-06 | 9.15E-09 | 0.92437539 | 580.6193896 | 0.06039455 | 1.123054912 |
| 0.001331297 | 7.55E-06 | 9.15E-09 | 0.92529047 | 574.6597388 | 0.063061347 | 1.068140779 |
| 0.0016864 | 8.58E-06 | 9.43E-09 | 0.92144921 | 487.5241828 | 0.063302956 | 1.369449952 |
| 0.001674623 | 8.60E-06 | 9.44E-09 | 0.92212895 | 470.7991599 | 0.063761386 | 1.318765154 |
| 0.001705639 | 8.60E-06 | 9.43E-09 | 0.92224627 | 501.266664 | 0.063720131 | 1.404108303 |
| 0.001661544 | 8.49E-06 | 9.41E-09 | 0.92094076 | 516.7860769 | 0.06203405 | 1.423653105 |
| 0.001651692 | 8.49E-06 | 9.40E-09 | 0.92242937 | 525.3939511 | 0.063093897 | 1.416156203 |
| 0.001707262 | 8.57E-06 | 9.42E-09 | 0.9221902 | 519.6306233 | 0.062828607 | 1.455547964 |
| 0.001700942 | 8.52E-06 | 9.40E-09 | 0.92300415 | 534.9026224 | 0.06708379 | 1.371545186 |
| 0.001711483 | 8.56E-06 | 9.42E-09 | 0.9211865 | 535.4263858 | 0.063420757 | 1.487295516 |
| 0.001687531 | 8.49E-06 | 9.41E-09 | 0.92052499 | 568.4805757 | 0.05985208 | 1.624230216 |
| 0.001706701 | 8.70E-06 | 9.45E-09 | 0.92293356 | 515.4529926 | 0.063367813 | 1.516038213 |
| 0.001808523 | 8.86E-06 | 9.49E-09 | 0.92459605 | 478.6794712 | 0.064631957 | 1.477405775 |
| 0.001804338 | 8.78E-06 | 9.46E-09 | 0.92384905 | 477.9505093 | 0.066595888 | 1.385363795 |
| 0.00177177 | 8.74E-06 | 9.46E-09 | 0.92246824 | 511.1719567 | 0.067497676 | 1.443988578 |

| | | | | | | |
|-------------|----------|----------|------------|-------------|-------------|-------------|
| 0.001724749 | 8.66E-06 | 9.45E-09 | 0.9206298 | 522.2599872 | 0.06251873 | 1.540589933 |
| 0.001734685 | 8.66E-06 | 9.45E-09 | 0.92085 | 490.8416089 | 0.059749809 | 1.519633464 |
| 0.001681351 | 8.58E-06 | 9.43E-09 | 0.92113789 | 534.240561 | 0.063373719 | 1.49647216 |
| 0.001709372 | 8.64E-06 | 9.45E-09 | 0.92004762 | 492.3265475 | 0.058613426 | 1.538520461 |
| 0.001489762 | 8.11E-06 | 9.28E-09 | 0.92152618 | 759.3296032 | 0.063744454 | 1.691157245 |
| 0.001481032 | 8.07E-06 | 9.26E-09 | 0.92228876 | 809.3734973 | 0.060784382 | 1.843675393 |
| 0.001500526 | 8.15E-06 | 9.29E-09 | 0.92243548 | 778.8044465 | 0.059952556 | 1.867636562 |
| 0.001457162 | 8.02E-06 | 9.26E-09 | 0.91943031 | 801.7191904 | 0.060931043 | 1.79757666 |
| 0.001483183 | 8.04E-06 | 9.26E-09 | 0.92087022 | 800.4700126 | 0.058746826 | 1.870257039 |
| 0.001476562 | 8.05E-06 | 9.25E-09 | 0.92281374 | 789.9278597 | 0.060489941 | 1.787167103 |
| 0.00145941 | 8.02E-06 | 9.24E-09 | 0.92237907 | 793.8235793 | 0.060932264 | 1.764052398 |
| 0.001480906 | 8.08E-06 | 9.26E-09 | 0.92305553 | 790.7435176 | 0.059803206 | 1.838938413 |
| 0.001466375 | 8.01E-06 | 9.24E-09 | 0.92086623 | 812.8740577 | 0.05666661 | 1.940033551 |

Appendix C-2: Images Features Data Set for Osteoporoticpatient

| COARSNESS | Contrast | Direction | Edge Pixels | Length of Edges | NUMBER OF EDGES | EDGE LENGTH |
|------------------|-----------------|------------------|--------------------|------------------------|------------------------|--------------------|
| 0.00194941 | 8.92E-06 | 9.51E-09 | 0.921203327 | 733.7945181 | 0.057212448 | 2.65867579 |
| 0.00192487 | 8.86E-06 | 9.49E-09 | 0.921641321 | 741.7864829 | 0.066177398 | 2.261544155 |
| 0.00193828 | 8.86E-06 | 9.49E-09 | 0.922488424 | 732.5324859 | 0.065029193 | 2.267902433 |
| 0.00194331 | 8.88E-06 | 9.48E-09 | 0.923721329 | 750.4922358 | 0.068027554 | 2.226979928 |
| 0.00198671 | 8.87E-06 | 9.48E-09 | 0.923649532 | 765.4570921 | 0.068001207 | 2.264665953 |
| 0.00195198 | 8.82E-06 | 9.47E-09 | 0.92410342 | 735.6311836 | 0.062208703 | 2.320603103 |
| 0.00197838 | 8.86E-06 | 9.48E-09 | 0.924544796 | 689.4980484 | 0.07033494 | 1.958801274 |
| 0.00203968 | 8.93E-06 | 9.49E-09 | 0.926066838 | 664.4857567 | 0.07033419 | 1.942940809 |
| 0.00197347 | 8.82E-06 | 9.48E-09 | 0.923751139 | 679.6065175 | 0.059482483 | 2.250352707 |
| 0.00192719 | 8.74E-06 | 9.46E-09 | 0.922519775 | 691.0633915 | 0.060993043 | 2.159573098 |
| 0.00338331 | 1.09E-05 | 9.76E-09 | 0.925246827 | 872.3580546 | 0.081692525 | 4.81965776 |
| 0.00343394 | 1.09E-05 | 9.77E-09 | 0.926965971 | 866.6417262 | 0.08189877 | 4.841573889 |
| 0.00350927 | 1.11E-05 | 9.78E-09 | 0.922945519 | 857.4576908 | 0.08248429 | 5.073714147 |
| 0.00337028 | 1.09E-05 | 9.77E-09 | 0.922137405 | 873.1499578 | 0.075631239 | 5.423291663 |
| 0.00343769 | 1.10E-05 | 9.77E-09 | 0.924030645 | 890.8284835 | 0.079536815 | 5.24016755 |
| 0.00335948 | 1.09E-05 | 9.77E-09 | 0.921148587 | 888.5469381 | 0.074749316 | 5.417969135 |
| 0.00205255 | 9.01E-06 | 9.51E-09 | 0.923762243 | 677.2150234 | 0.075137529 | 1.934900067 |
| 0.00215195 | 9.11E-06 | 9.53E-09 | 0.925994938 | 679.5262588 | 0.074310983 | 2.034509757 |
| 0.00212324 | 9.07E-06 | 9.53E-09 | 0.923255236 | 628.282182 | 0.074178326 | 1.869887446 |
| 0.00210419 | 9.05E-06 | 9.52E-09 | 0.923673503 | 658.3053675 | 0.071875256 | 2.000928169 |
| 0.00217063 | 9.09E-06 | 9.53E-09 | 0.923846581 | 636.0090044 | 0.076931629 | 1.838176313 |
| 0.00211722 | 9.04E-06 | 9.52E-09 | 0.924262989 | 653.5470141 | 0.069276291 | 2.048736721 |
| 0.0020547 | 8.96E-06 | 9.51E-09 | 0.922184732 | 627.8009064 | 0.071488823 | 1.851920078 |
| 0.00209861 | 9.02E-06 | 9.51E-09 | 0.925582641 | 646.7024171 | 0.07822127 | 1.771787444 |
| 0.00205602 | 8.97E-06 | 9.51E-09 | 0.92384585 | 641.3446647 | 0.073444693 | 1.837663796 |
| 0.00227323 | 9.25E-06 | 9.57E-09 | 0.921326787 | 594.331969 | 0.068015806 | 2.092718201 |

| | | | | | | |
|------------|----------|----------|-------------|-------------|-------------|-------------|
| 0.00227248 | 9.24E-06 | 9.57E-09 | 0.921322146 | 612.7347969 | 0.067600251 | 2.165140625 |
| 0.00222562 | 9.19E-06 | 9.56E-09 | 0.921740651 | 594.3453283 | 0.062724067 | 2.209462187 |
| 0.00220645 | 9.16E-06 | 9.56E-09 | 0.921721606 | 562.2887763 | 0.064948899 | 1.993931831 |
| 0.00222764 | 9.16E-06 | 9.56E-09 | 0.920944736 | 534.6674214 | 0.06837212 | 1.806308856 |
| 0.00223389 | 9.18E-06 | 9.55E-09 | 0.923005727 | 536.9883977 | 0.073349916 | 1.693969709 |
| 0.00274824 | 1.01E-05 | 9.67E-09 | 0.925827815 | 1036.807859 | 0.08013245 | 4.284329995 |
| 0.00267157 | 9.98E-06 | 9.67E-09 | 0.924661945 | 978.8298034 | 0.072440438 | 4.350354682 |
| 0.0026878 | 1.00E-05 | 9.68E-09 | 0.923502154 | 936.5799945 | 0.075441021 | 4.036982735 |
| 0.00266944 | 9.95E-06 | 9.67E-09 | 0.922350682 | 948.2198031 | 0.066567988 | 4.558749053 |
| 0.00283826 | 1.01E-05 | 9.69E-09 | 0.923760684 | 900.2804091 | 0.067692308 | 4.546870753 |
| 0.00260765 | 9.84E-06 | 9.65E-09 | 0.923605543 | 943.2373109 | 0.070858626 | 4.065678064 |
| 0.00197112 | 9.22E-06 | 9.57E-09 | 0.920143735 | 766.2404264 | 0.062245716 | 2.92458178 |
| 0.00194243 | 9.17E-06 | 9.56E-09 | 0.921425878 | 781.5487197 | 0.063578618 | 2.85236759 |
| 0.00195733 | 9.11E-06 | 9.55E-09 | 0.920640308 | 764.2419136 | 0.066972114 | 2.581898357 |
| 0.00206075 | 9.29E-06 | 9.58E-09 | 0.921689317 | 697.4336456 | 0.066792614 | 2.545378269 |
| 0.00204337 | 9.24E-06 | 9.57E-09 | 0.920614942 | 714.9677191 | 0.06281279 | 2.728884424 |
| 0.0020989 | 9.31E-06 | 9.58E-09 | 0.922926112 | 735.4763401 | 0.065923294 | 2.734112788 |
| 0.00203944 | 9.21E-06 | 9.56E-09 | 0.923554748 | 761.6225486 | 0.066336547 | 2.691245755 |
| 0.00200896 | 9.18E-06 | 9.56E-09 | 0.923840868 | 764.6524175 | 0.062128298 | 2.842574043 |
| 0.00201312 | 9.19E-06 | 9.56E-09 | 0.923344948 | 745.9103815 | 0.067595819 | 2.563265916 |
| 0.00184883 | 8.90E-06 | 9.51E-09 | 0.920582464 | 715.9646904 | 0.061138077 | 2.41879963 |
| 0.00207634 | 9.23E-06 | 9.56E-09 | 0.922649484 | 663.9532375 | 0.069045015 | 2.273812457 |
| 0.00222893 | 9.67E-06 | 9.63E-09 | 0.923087894 | 822.5660511 | 0.068461401 | 3.427358546 |
| 0.00223297 | 9.67E-06 | 9.63E-09 | 0.924732706 | 790.5390184 | 0.071372938 | 3.137059597 |
| 0.00222853 | 9.61E-06 | 9.63E-09 | 0.922756031 | 783.1048214 | 0.062851978 | 3.465065582 |
| 0.00266848 | 9.61E-06 | 9.61E-09 | 0.925549157 | 679.6403301 | 0.076140557 | 2.462464964 |
| 0.00269439 | 9.66E-06 | 9.62E-09 | 0.924530963 | 645.6509001 | 0.082381154 | 2.21113322 |

| | | | | | | |
|------------|----------|----------|-------------|-------------|-------------|-------------|
| 0.0025971 | 9.54E-06 | 9.61E-09 | 0.922412047 | 616.1476795 | 0.073468837 | 2.265248822 |
| 0.00263231 | 9.63E-06 | 9.62E-09 | 0.925924642 | 613.8741252 | 0.077922978 | 2.184605428 |
| 0.00263231 | 9.63E-06 | 9.62E-09 | 0.925924642 | 613.8741252 | 0.077922978 | 2.184605428 |
| 0.0025538 | 9.54E-06 | 9.61E-09 | 0.925564613 | 627.7598958 | 0.071361753 | 2.351160659 |
| 0.00272203 | 9.70E-06 | 9.63E-09 | 0.923708371 | 718.1699376 | 0.06970297 | 2.96764437 |
| 0.0026366 | 9.64E-06 | 9.62E-09 | 0.92435857 | 704.2111696 | 0.070285974 | 2.80562219 |
| 0.00205758 | 9.22E-06 | 9.56E-09 | 0.922179332 | 655.3478608 | 0.067654772 | 2.283442024 |